Received: 11 July 2021 | Revised: 5 January 2022 | Accepted: 15 March 2022

DOI: 10.1002/rnc.6141

RESEARCH ARTICLE

WILEY

Robust decoupling of uncertain subsystems

Tamás Baár | **Tamás Luspay**

Systems and Control Lab, Institute for Computer Science and Control (SZTAKI), Eötvös Loránd Research Network (ELKH), Budapest, Hungary

Correspondence
Tamás Baár, Systems and Control Lab, Institute for Computer Science and Control (SZTAKI), Eötvös Loránd Research Network (ELKH), Kende u. 13-17. 1111. Budapest, Hungary.
Email: baartamas@sztaki.hu

Funding information
European Unions Horizon 2020, Grant/Award Number: No. 815058; Hungarian Ministry of Innovation and Technology NRDI Office

Abstract

The article presents a robust subsystem decoupling framework for uncertain linear systems with linear fractional representation, where the uncertainties are described by Integral Quadratic Constraints. The proposed method relies on the synthesis of input- and output transformations, which maximize the robust excitation of a selected subsystem, while minimize this effect on the other parts of the dynamics. More precisely, the notion of minimum gain is defined (and discussed) for uncertain systems, which is then maximized for the targeted subsystem. In order to achieve decoupling, the maximum sensitivity of the undesired dynamical part is minimized simultaneously. These criteria lead to an optimization problem subject to linear matrix inequality constraints, hence can be effectively solved. Numerical examples are used for demonstrating the developed method and its possible applications.

KEYWORDS

IQC, LFT, LMI, robust minimum sensitivity, subsystem decoupling

1 | INTRODUCTION

The article discusses a decoupling method for linear uncertain systems, which allows to control subsystems without interacting with other parts of the dynamics. The problem is best understood based on the general state space form of a linear time invariant (LTI) system given as

$$\begin{aligned} \dot{x}(t) &= Ax(t) + Bu(t), \\ y(t) &= Cx(t) + Du(t), \end{aligned} \tag{1}$$

with the standard notations of $x \in \mathbb{R}^{n_x}$, $u \in \mathbb{R}^{n_u}$, and $y \in \mathbb{R}^{n_y}$ being the state-, input-, and output- vectors, respectively. We assume that the system is given (or transformed) in the following subsystem form[*]:

$$\begin{aligned} A &= \begin{bmatrix} A_c & 0 \\ 0 & A_d \end{bmatrix}, \quad B = \begin{bmatrix} B_c \\ B_d \end{bmatrix}, \\ C &= \begin{bmatrix} C_c & C_d \end{bmatrix}, \quad D = \begin{bmatrix} D \end{bmatrix}. \end{aligned} \tag{2}$$

Here, subscripts are referring to the subsystems which are aimed to be *c*ontrolled, or *d*ecoupled. An immediate observation of the structure (2) is that the two subsystems are coupled through only their input–output channels. In order to isolate the two subsystems from each other, it is natural to seek for input and output transformations which weakens or resolves

this coupling. As it is shown in Section 2 this can be achieved by taking the linear combinations of the input and output signals, respectively. The optimal combinations are termed as blend vectors, and they are calculated by an linear matrix inequality (LMI) based optimization program. The results reported in the article are the extensions of the methodology developed for nominal systems' decoupling,[1] and the two main contributions are:

1. **Extending the notion of minimum sensitivity to uncertain linear systems.** Relying on the work of References 2 and 3 an analysis condition with a corresponding LMI formulation (relying on Integral Quadratic Constraints (IQCs)) is provided. By the aid of the Generalized Kalman-Yakubovich-Popov lemma, the finite frequency version of the underlying analysis condition is also discussed.
2. **Robust subsystem decoupling.** By building on the LMI formulation of the robust minimum sensitivity and the well known worst-case gain, an LMI based robust subsystem decoupling approach is presented. It is the robust extension of the method presented in Reference 1, and it relies on the synthesis of input- and output transformation vectors which guarantee robust decoupling of the subsystems. By building on the IQC framework, the proposed method is able to handle various types of uncertainties.

The outlined idea of subsystem decoupling points towards the recent trends of structured controller design, where each block of the controller may correspond to a specific subsystem. A conventional decoupling methodology in the control system literature is the so called input–output decoupling, which is a frequently used approach to simplify the control system design by enforcing a diagonal controller structure. This is a well established research field,[4] and most approaches trace back to the application of a suitable method which converts the system into a diagonally dominant one (such as: decoupling by static and dynamic pre- and post-compensators,[5,6] decoupling by state feedback,[7] etc.). A common feature is that the outputs are defined to be the controlled variables. These methods limit the interaction between certain loops, and consequently open up the possibility to design a feedback controller with diagonal structure, where each diagonal block in the controller's transfer function matrix is responsible for controlling one output. However, it has been noted[7] that these methods are very sensitive to modeling errors and plant uncertainties.

Accordingly, attempts for robust decoupling have also gained attention in the control community. Among the several methods in the literature, we only highlight the one presented in chap. 8 of Reference 7, since it relies on similar mathematical tools as the approach presented in the article. Namely, a LMI based robust state feedback design approach for uncertain systems is presented in Reference 7, which results in a diagonally dominant closed-loop plant. The method relies on the LMI description of the minimum and maximum gains of a dynamical system; the designed state feedback maximizes the transfer through the diagonal term of the closed loop transfer function matrix, and minimizes the maximum sensitivities over the off diagonal terms. Due to the presence of uncertainties exact decoupling is not possible, hence Reference 7 labels this approach as near decoupling. The resulting transfer function matrix is diagonally dominant, with transfer functions between each controlled variable and a corresponding set of control inputs on its diagonal. However (2) reveals that due to their additive nature, various subsystems may contribute to a given system output. In contrast to this approach, we aim to design transformations which turn the plant into diagonally dominant such that each diagonal entry corresponds a certain dynamic subsystem.

Another main direction in decoupled control design is the approach of controlling selected subsystems by a specific control law. Here, the frequency-wise separation of the different subsystems is one well-known tool. Traditionally notch-, or roll-off filters are introduced to suppress certain frequency ranges, limiting the controller's interaction with various parts of the dynamics.[8,9] In this framework, an $\mathcal{H}_\infty$ closed-loop shaping approach has been presented in Reference 10, involving band-stop weighting functions to achieve decoupled interaction between the plant and the controller. The concept of dynamic filters often leads to satisfactory results, however the dimension of the controller is increased by each applied weighting filter. In addition, the method was shown to provide satisfactory robustness properties against input and output multiplicative uncertainties.

Our approach fits more closely into a recently developed trend in the decoupled control design; which is decoupling by means of suitable input and output transformations. The advantage of these approaches is the unaltered dimension of the underlying control problem: the static transformations convert the design to a SISO problem. The method of "Modal Isolation and Damping for Adaptive Aeroelastic Suppression" (MIDAAS)[11] is a constrained least-squares optimization based algorithm, which designs controller for specifically damping the undesired dynamical components in the system, without affecting the remaining dynamics. For this purposes a special combination of the available input- and output signals are used. Its application to aerospace problem has been revealed by successful flutter suppression without

interacting with the aircraft's rigid body dynamics. Another static decoupling approach is presented in References 12 and 13 which relies on a joint $\mathcal{H}_2$ norm based input- and output-blend calculation method to maximize the controllability and observability of the selected modes and accordingly facilitates their decoupled control. The method has been successfully applied in a gust load alleviation system on an experimental flexible wing,[14] and in a structured controller design of a flexible wing flutter demonstrator aircraft, suppressing unstable wing oscillations.[15] Despite their successful applications, these methods do not have robust extensions for uncertain systems.

The present paper addresses the problem of subsystem decoupling of uncertain dynamics by input- and output transformations and organized as follows. The robust decoupling problem (RDP) is formalized in Section 2, followed by the necessary mathematical backgrounds in Section 3. Section 4 extends the minimum sensitivity analysis to uncertain systems, relying on an IQC based description of the uncertainties. This section is the first novel contribution of the article. The second new contribution is the design of the robust decoupling transformations, as discussed in Section 5, with the numerical algorithms included in the Appendix. Numerical results are reported in Section 6, while concluding remarks and open research questions are closing the article in Section 7.

2 | THE ROBUST DECOUPLING PROBLEM

2.1 | Notations

The mathematical notations of the article are fairly standard. $\mathbb{R}$ and $\mathbb{C}$ denote the set of real and complex numbers, respectively. $\mathbb{RL}_\infty$ is the set of rational transfer functions with real coefficients that are proper and have no poles on the imaginary axis. $\mathbb{RH}_\infty$ is the subset of functions in $\mathbb{RL}_\infty$ that are analytic in the closed right half complex plane. $\mathbb{R}^{m\times n}$, $\mathbb{C}^{m\times n}$, $\mathbb{RL}_\infty^{m\times n}$, $\mathbb{RH}_\infty^{m\times n}$ denote the sets of $m\times n$ matrices that are in $\mathbb{R}$, $\mathbb{C}$, $\mathbb{RL}_\infty$, and $\mathbb{RH}_\infty$, respectively. The n dimensional identity matrix is denoted by I_n.

Furthermore $y\in\mathcal{L}_2$ if $||y||_2^2=\int_0^\infty |y(t)|^2dt<\infty$, and $y\in\mathcal{L}_{2e}$ if $||y||_2^2=\int_0^\infty |y_T(t)|^2dt<\infty$, $T\in\mathbb{R}^+$, with $y_T(t)=y(t)$ for $0\le t\le T$ and $y_T(t)=0$ for $t\ge T$.

Systems will be denoted by capital caligraphic letters ($\mathcal{M}$) or the two Greek letters Π, Ψ (in order to follow the conventions of the literature), matrices are written by math variables (M). Furthermore, $M\prec 0$ ($\preccurlyeq$) and $M\succ 0$ ($\succcurlyeq$) denote the negative- and positive (semi)definiteness of matrix M, respectively. For $M\in\mathbb{C}^{m\times n}$, M^T denotes the transpose, and M^* denotes the complex conjugate transpose. S^m denotes the set of a symmetric $m\times m$ matrices. The symmetric terms in quadratic matrix products are replaced by $\left[\star\right]$. The imaginary unit is denoted by j. The para-Hermitian conjugate of $\mathcal{M}\in\mathbb{RL}_\infty^{m\times n}$ is denoted as $\mathcal{M}^\sim$ and defined by $\mathcal{M}^\sim(s):=\mathcal{M}(-s)^T$, with s being the Laplace variable. Lastly, the dual of an $\mathcal{M}(A,B,C,D)$ state space system is defined by $\mathcal{M}^T(A^T,C^T,B^T,D^T)$.

2.2 | The robust decoupling problem

Before going into the details in the forthcoming sections, first an overview of the RDP is given.

Throughout the article the uncertain system is assumed to be given as the linear fractional (LFT) interconnection of a known certain part $\mathcal{M}$ and an unknown, but norm bounded, structured uncertainty set $\Delta\in\mathbf{\Delta}$. This standard representation is denoted by $\mathcal{F}_u(\mathcal{M},\Delta)$ and shown in Figure 2. Similarly for the nominal case presented in (2), we suppose that system $\mathcal{M}$ is brought to a subsystem form with $\mathcal{M}=\mathcal{M}_c+\mathcal{M}_d$. The indices are denoting that the subsystems should be controlled, or decoupled, respectively.

In the article, the decoupling of these two subsystems is characterized by the minimum and maximum sensitivities, defined as

$$||\mathcal{M}_C||_{\Delta-}=\inf_{\Delta\in\mathbf{\Delta}}||\mathcal{F}_u(\mathcal{M}_C,\Delta)||, \tag{3}$$

$$||\mathcal{M}_D||_{\Delta\infty}=\sup_{\Delta\in\mathbf{\Delta}}||\mathcal{F}_u(\mathcal{M}_D,\Delta)||. \tag{4}$$

The $||\mathcal{M}||_{\Delta\infty}$ term is usually labeled in the literature as the worst-case gain of the $\mathcal{F}_u(\mathcal{M},\Delta)$ interconnection.[5] As it can be depicted from its definition, we are using this metric for the subsystem which has to be decoupled, while the minimum

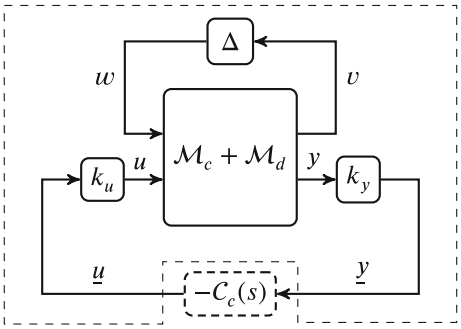

FIGURE 1 Closed loop control scheme with input and output blending

gain is used for the targeted subsystem (see Equation 3) and discussed in Section 4. Accordingly, we will often refer to $||\mathcal{M}||_{\Delta\infty}$ as the robust maximum gain. Note also the subscript Δ in the above definitions, explicitly indicating that these metrics are computed over the uncertainty set.

It is well known from the analysis of uncertain systems that the available knowledge regarding the perturbation block Δ has a great importance. Generally, the exact description of Δ is unknown, nevertheless, some assumptions can be given. Then (3) and (4) have to be evaluated over all the possible uncertainties satisfying the assumptions. Among the different uncertainty modeling formalism, the IQC based framework has proved to cover a large class of uncertainties and therefore used in the article. Appendix A discusses the IQC-based robust maximum gain calculation using an LMI-based optimization. At the same time, the computation of the robust minimum gain (3) is not yet discussed in the literature, (except Reference 16) and covered in Section 4, as a contribution of the article.

Now, based on Figure 1, the decoupling problem can be stated as follows. Design an environment (denoted by the dashed frame) which allows the control of the subsystem $\mathcal{M}_c(s)$ by a corresponding controller $C_c(s)$ and minimizes the interaction with $\mathcal{M}_d(s)$[†]. This is achieved by finding linear combinations of the input- and output-signals of the system, respectively. For this purpose $k_u \in \mathbb{R}^{n_u \times 1}$ and $k_y \in \mathbb{R}^{n_y \times 1}$ are introduced: the normalized (i.e., $\|k_u\| = \|k_y\| = 1$) input- and output-blending vectors. They transform the signal vectors u and y onto a single dimension, reducing the analysis and synthesis problems into a SISO one from $\underline{u}$ to $\underline{y}$. In Figure 1 the control input $\underline{u} \in \mathbb{R}$ is distributed between the plant's inputs ($u = k_u \underline{u}$) in a way that they excite the subsystem which one wishes to control as much as possible, without exciting the remaining dynamics (to be decoupled). Similarly the controller's input $\underline{y} = k_y^T y \in \mathbb{R}$ is calculated such that the information content from the targeted subsystem is maximized, while from the other subsystems is minimized. The problem involving subsystem sensitivity measures is then formalized as follows.

Problem 1. The robust decoupling problem (RDP). Find normalized vectors k_u and k_y such that they maximize the transfer through the controlled subsystem

$$\begin{aligned} &\max_{k_u,k_y}: \quad \beta \\ &\text{s.t.:} \quad ||k_y^T \mathcal{M}_c k_u||_{\Delta-}^{[\underline{\omega},\overline{\omega}]} > \beta, \quad \beta \geq 0, \end{aligned} \tag{5}$$

and simultaneously minimize the amplification of the remaining subsystem, so

$$\begin{aligned} &\min_{k_u,k_y}: \quad \gamma \\ &\text{s.t.:} \quad ||k_y^T \mathcal{M}_d k_u||_{\Delta\infty} < \gamma, \quad \gamma \geq 0, \end{aligned} \tag{6}$$

for all $\Delta \in \mathbf{\Delta}$. Here β and γ are two non-negative scalars denoting the robust minimum and maximum sensitivities of the subsystems[‡].

3 | MATHEMATICAL BACKGROUND

3.1 | Integral Quadratic Constraints

Among the different uncertainty handling methodologies, the IQC based framework received the most attention, due to the fact that numerous dynamical components (e.g., norm-bounded or polytopic uncertainties, time delays, saturation, various types of non-linearities, etc.) can be covered by this formalism. The standard interconnection of a nominal, known dynamics and an uncertain block is given in Figure 2, known as the linear fractional representation. Throughout the article we are only interested in well-posed LFT formulations for $\mathcal{M} = \begin{bmatrix} \mathcal{M}_{11} & \mathcal{M}_{12} \\ \mathcal{M}_{21} & \mathcal{M}_{22} \end{bmatrix}$, where $(I - \mathcal{M}_{11}\Delta)^{-1}$ is nonsingular and so the transfer from the input to the output is uniquely defined as

$$y = \left(\mathcal{M}_{21}\Delta(I - \mathcal{M}_{11}\Delta)^{-1}\mathcal{M}_{12} + \mathcal{M}_{22}\right) u. \tag{7}$$

The IQC framework assumes that the input and output signals of the uncertainty block satisfy an integral formula. We follow the terminology of Reference 2, but the interested reader is referred to References 17,18 for a more detailed presentation and discussion about the theory of IQCs.

We say that the signals $v \in \mathcal{L}_2^{n_v}$, $w \in \mathcal{L}_2^{n_w}$ in the interconnection depicted in Figure 3 are satisfying the IQC defined by Π in the frequency domain, if

$$\int_{-\infty}^{\infty} \begin{bmatrix} \hat{v}(j\omega) \\ \hat{w}(j\omega) \end{bmatrix}^* \Pi(j\omega) \begin{bmatrix} \hat{v}(j\omega) \\ \hat{w}(j\omega) \end{bmatrix} d\omega \leq 0, \tag{8}$$

where $\hat{v}$ and $\hat{w}$ are the Fourier transforms of v, and w respectively. A time-domain alternative is constructed by calculating a $(\Psi,\ M)$ factorization of Π (with $\Pi = \Psi^{\sim} M \Psi$), where $M \in \mathrm{S}^{n_z}$ and $\Psi \in \mathbb{RH}_\infty^{n_z \times (n_v + n_w)}$ is a stable, invertible, linear system with the following frequency domain realization:

$$\Psi(j\omega) := C_\Psi (j\omega I - A_\Psi)^{-1} \begin{bmatrix} B_{\Psi_v} & B_{\Psi_w} \end{bmatrix} + \begin{bmatrix} D_{\Psi_v} & D_{\Psi_w} \end{bmatrix}, \tag{9}$$

and state-space representation:

$$\begin{aligned} \dot{x}_\Psi &= A_\Psi x_\Psi(t) + B_{\Psi_v} v(t) + B_{\Psi_w} w(t), \\ z(t) &= C_\Psi x_\Psi(t) + D_{\Psi_v} v(t) + D_{\Psi_w} w(t). \end{aligned} \tag{10}$$

This $(\Psi,\ M)$ factorization allows the frequency domain IQC condition (8) to be expressed in the time domain as

$$\int_0^T z(t)^T M z(t) dt \geq 0. \tag{11}$$

If $T = \infty$ then $(\Psi,\ M)$ is called a soft factorization. As Reference 2 discusses the formulation of an IQC as a time-domain inequality (Equation 11) is only valid for frequency domain IQCs that admit a hard factorization $(\Psi,\ M)$, where (11) holds for all $T \geq 0$.

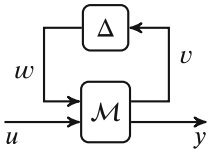

FIGURE 2 LFT description of an uncertain system

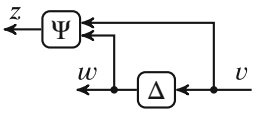

FIGURE 3 Graphical interpretation of an IQC

The remainder of the article will simply treat $(\Psi,\ M)$ as a hard factorization, and when Δ satisfies an IQC constraint given by $(\Psi,\ M)$, then it will be denoted by $\Delta \in \mathrm{IQC}(\Psi,\ M)$. Note that there are infinitely many hard factorizations for Π, among them a special class is called the J-spectral factorization.[19] This is a straightforward way for finding hard factorizations for dynamic IQC filters.

Definition 1. The J-spectral factorization.[19] $(\hat{\Psi}, J_{n_v,n_w})$ is called a J_{n_v,n_w} spectral factor of $\Pi = \Pi^{\sim} \in \mathbb{RL}_{\infty}^{(n_v+n_w)\times(n_v+n_w)}$ if $\Pi = \hat{\Psi}^{\sim} J_{n_v,n_w} \hat{\Psi}, J_{n_v,n_w} = \begin{bmatrix} I_{n_v} & 0 \\ 0 & -I_{n_w} \end{bmatrix}$, and $\hat{\Psi}, \hat{\Psi}^{-1} \in \mathbb{RH}_{\infty}^{(n_v+n_w)\times(n_v++n_w)}$.

This J-spectral factorization always exists, if Π satisfies the positive-negative multiplier property.

Definition 2. Positive-negative (PN) multiplier.[19] Let $\Pi = \Pi^{\sim} \in \mathbb{RL}_{\infty}^{(n_v+n_w)\times(n_v+n_w)}$ be partitioned as $\begin{bmatrix} \Pi_{11} & \Pi_{12} \\ \Pi_{12}^{\sim} & \Pi_{22} \end{bmatrix}$, where $\Pi_{11} \in \mathbb{RL}_{\infty}^{n_v\times n_v}$ and $\Pi_{22} \in \mathbb{RL}_{\infty}^{n_w\times n_w}$. Π is said to be a strict positive-negative (PN) multiplier if $\Pi_{11} > 0$ and $\Pi_{22} < 0\ \forall \omega \in \mathbb{R} \cup \{\infty\}$.

At J-spectral factorizations the matrix J is diagonal and $\hat{\Psi}$ is square, stable and stably invertible. Furthermore J-spectral factorizations exist for all strict PN multipliers.[18] The $\Pi = \hat{\Psi}^{\sim} J_{n_v,n_w} \hat{\Psi}$ J-spectral factorizations satisfy the

$$\int_0^T z(t)^T J_{n_v,n_w} z(t) dt \geq 0, \tag{12}$$

integral relationship, that is, it is a hard factorization. In addition, if Δ satisfies an IQC constraint given by its J-spectral factorization $\left(\hat{\Psi},\ J\right)$, then it will be denoted by $\Delta \in \mathrm{IQC}\left(\hat{\Psi},\ J\right)$. Hard and soft IQC factorizations are discussed in depth in References 17 and 18.

3.2 | Dual Integral Quadratic Constraints

System duality plays a key role in the proposed decoupling algorithm, therefore the dual IQCs are introduced briefly, based on the discussion in Reference 19.

Definition 3. The dual IQC multiplier.[19] Given the strict PN primal IQC multiplier $\Pi = \Pi^{\sim} \in \mathbb{RL}_{\infty}^{(n_v+n_w)\times(n_v+n_w)}$, the dual IQC multiplier is denoted by $\boldsymbol{D}(\Pi) \in \mathbb{RL}_{\infty}^{(n_w+n_v)\times(n_w+n_v)}$ and is defined as

$$\boldsymbol{D}(\Pi) := \begin{bmatrix} 0 & -I_{n_w} \\ I_{n_v} & 0 \end{bmatrix} \Pi^{-T} \begin{bmatrix} 0 & -I_{n_v} \\ I_{n_w} & 0 \end{bmatrix}. \tag{13}$$

Here, Π^{-T} is the transpose of the inverse of Π. The definition assumes Π to be a strict PN multiplier with $\Pi_{11} \succ 0$ and $\Pi_{22} \prec 0\ \forall \omega \in \mathbb{R} \cup \{\infty\}$, therefore Π^{-1} and $\boldsymbol{D}(\Pi)$ exist. Definition 3 can also be extended for the case when Π is given by its stable (Ψ, M) factorization. Then by Definition 3, the dual IQC multiplier can be expressed as

$$\boldsymbol{D}(\Pi) = \begin{bmatrix} 0 & -I_{n_w} \\ I_{n_v} & 0 \end{bmatrix} \Psi^{-T\sim} M^{-1} \Psi^{-T} \begin{bmatrix} 0 & -I_{n_v} \\ I_{n_w} & 0 \end{bmatrix}, \tag{14}$$

from which it follows that

$$\boldsymbol{D}(\Pi) = \boldsymbol{D}(\Psi)^{\sim} M \boldsymbol{D}(\Psi), \text{ where } \boldsymbol{D}(\Psi) = \begin{bmatrix} 0 & -I_{n_w} \\ I_{n_v} & 0 \end{bmatrix} \Psi^{-T} \begin{bmatrix} 0 & -I_{n_v} \\ I_{n_w} & 0 \end{bmatrix}. \tag{15}$$

Finally, the connections between the primal and the dual representations are discussed in Lemma 1,[19] and are illustrated in Figure 4.

Lemma 1. *The dual uncertain system.*[19] *Given $\mathcal{M}$ and Π, the following statements hold.*

1. *$\mathcal{M}$ is quadratically stable if and only if its dual $\mathcal{M}^T$ is quadratically stable.*
2. *Π is a strict PN multiplier if and only if $\boldsymbol{D}(\Pi)$ is a strict PN multiplier.*

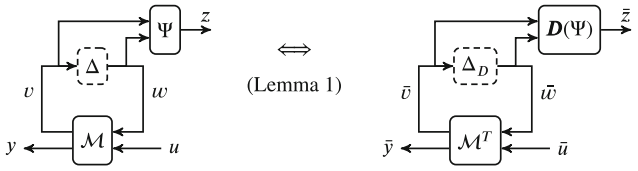

FIGURE 4 Relationship between the nominal and dual IQC representations

3. *The $\mathcal{F}_u(\mathcal{M},\Delta)$ and $\mathcal{F}_u(\mathcal{M}^T,\Delta_D)$ representations of the uncertain system (shown in Figure 4) have the same maximum sensitivity.*
4. *Let (Ψ,M) be any stable factorization of Π and (Ψ_D,M_D) be any stable factorization of $\boldsymbol{D}(\Pi)$. Denote the maximum sensitivity analysis condition in (A1) by LMI$_{\Delta\infty}$. Then, $\exists P\in \mathrm{S}^{n_x}$ satisfying $\mathrm{LMI}_{\Delta\infty}(\mathcal{M},P,\gamma,\Psi,M)\prec 0$ if and only if $\exists P_D\in \mathrm{S}^{n_x}$ satisfying $\mathrm{LMI}_{\Delta\infty}(\mathcal{M}^T,P_D,\gamma,\Psi_D,M_D)\prec 0$.*

Proof. The proof can be found in Reference 19. ∎

4 | ROBUST MINIMUM SENSITIVITY

Having discussed the necessary mathematical tools, now we turn our focus on the computation of the robust minimum gain. In the article we will adopt a notion from the fault detection filtering literature to characterize the minimum sensitivity of a system (see e.g., References 20 and 21). More precisely we will use the so called $\mathcal{H}_-$ index, defined as

$$||\mathcal{G}(s)||_-^{[0,\overline{\omega}]} := \inf_{\omega\in[0,\overline{\omega}]} \underline{\sigma}\left[\mathcal{G}(j\omega)\right], \tag{16}$$

with $\underline{\sigma}$ denoting the minimum singular value and $\overline{\omega}$ being the maximal frequency value of the frequency band $[0,\overline{\omega}]$. The computation of the $\mathcal{H}_-$ index over an infinite frequency range can be written as a semi-definite optimization problem. Alternatively, the authors in Reference 3 proposed the following definition for the minimum gain:

Definition 4. Minimum gain of a system. A causal system $\mathcal{G}:\mathcal{L}_{2e}\to\mathcal{L}_{2e}$, has minimum gain $0\le\beta\le\infty$ if there exists ν, depending only on the initial conditions, such that

$$||\mathcal{G}u||_{2T}-\beta||u||_{2T}\ge\nu,\ \forall u\in\mathcal{L}_{2e},\ \forall T\in\mathbb{R}^+. \tag{17}$$

For LTI systems, an LMI-based computation has also been derived in Reference 3, which is referred as the "minimum gain lemma":

Lemma 2. *The calculation of the minimum gain.*[3] *A nominal LTI system given with state space matrices A, B, C, D has minimum gain $0\le\beta\le\infty$ if there exists $P\in \mathrm{S}^{n_x}\succcurlyeq 0$ such that*

$$\begin{bmatrix} PA+A^TP-C^TC & PB-C^TD \\ (PB-C^TD)^T & \beta^2I-D^TD \end{bmatrix} \preccurlyeq 0. \tag{18}$$

Proof. The detailed proof can be found in Reference 3 and hence is omitted here. ∎

This section discusses the IQC based robust minimum sensitivity calculation for uncertain LTI systems. The results can be interpreted as the robust extension of the minimum gain lemma presented in Reference 3 for LTI systems. Furthermore note that the discussion follows the results presented in Reference 2 corresponding to the robust maximum gain calculation.

4.1 | Robust minimum sensitivity over infinite frequency range

The system interconnection used for the analysis is shown in Figure 5, where the dashed frame denotes that Δ is removed from the interconnection and the Ψ filter is used to describe its effect. The state-space form corresponding to the extended

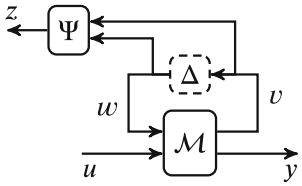

FIGURE 5 Analysis interconnection structure

dynamics is given by

$$\begin{aligned}\dot{\tilde{x}} &= \tilde{A}\tilde{x} + \tilde{B}_w w + \tilde{B}_u u,\\ \tilde{z} &= \tilde{C}_z\tilde{x} + \tilde{D}_{zw} w + \tilde{D}_{zu} u,\\ y &= \tilde{C}_y\tilde{x} + \tilde{D}_{yw} w + \tilde{D}_{yu} u,\end{aligned} \tag{19}$$

where the $\tilde{x} = \begin{bmatrix} x_{\mathcal{M}}^T & x_{\Psi}^T \end{bmatrix}^T$ state vector is composed of the states of the system $\mathcal{M}$ and the filter Ψ. The signal w is treated as an external signal and (11) is used for describing the $w = \Delta(v)$ relationship. Then, the following theorem provides the computation of the robust minimum gain over the entire frequency domain.

Theorem 1. *The robust minimum gain over the entire frequency domain. Assume that $\mathcal{F}_u(\mathcal{M}, \Delta)$ is well posed for all $\Delta \in$ IQC(Ψ, M). Then the minimum gain is finite and larger than β, if there exists a $P \in \mathbb{S}^{n_x}$ and $\lambda > 0$ such that*

$$\begin{bmatrix} P\tilde{A} + \tilde{A}^T P & P\tilde{B}_w & P\tilde{B}_u \\ \tilde{B}_w^T P & 0 & 0 \\ \tilde{B}_u^T P & 0 & \beta^2 I \end{bmatrix} + \lambda \begin{bmatrix} \tilde{C}_z^T \\ \tilde{D}_{zw}^T \\ \tilde{D}_{zu}^T \end{bmatrix} M \begin{bmatrix} \star \end{bmatrix} - \begin{bmatrix} \tilde{C}_y^T \\ \tilde{D}_{yw}^T \\ \tilde{D}_{yu}^T \end{bmatrix} \begin{bmatrix} \star \end{bmatrix} \prec 0. \tag{20}$$

is satisfied.

Proof. We start with the definition of the minimum gain (see Definition 4):

$$||\mathcal{M}u||_{2T} - \beta||u||_{2T} \geq \nu,\ \forall u \in \mathcal{L}_{2e},\ \forall T \in \mathbb{R}^+, \tag{21}$$

where the left-hand side can be rewritten as

$$||y||_{2T}^2 - \beta^2||u||_{2T}^2 = \int_0^T \left(|y|^2 - \beta^2|u|^2\right) dt. \tag{22}$$

The integral term in (22) can be trivially extended with a quadratic storage function and IQC term as:

$$\int_0^T \left(|y|^2 - \beta^2|u|^2 + \frac{d}{dt}(x^T P x) - \frac{d}{dt}(x^T P x) + \lambda z^T M z - \lambda z^T M z\right) dt. \tag{23}$$

Using the state-space representation in (19), the following form can be derived after some algebraic manipulations:

$$\int_0^T \begin{bmatrix} x \\ w \\ u \end{bmatrix}^T (-\Gamma_1 - \lambda\Gamma_2 + \Gamma_3 - \Gamma_4) \begin{bmatrix} x \\ w \\ u \end{bmatrix} dt + \int_0^T \begin{bmatrix} x \\ w \\ u \end{bmatrix}^T (\Gamma_1 + \lambda\Gamma_2) \begin{bmatrix} x \\ w \\ u \end{bmatrix} dt, \tag{24}$$

where we have introduced the following notations:

$$\Gamma_1 = \begin{bmatrix} P\tilde{A} + \tilde{A}^T P & P\tilde{B}_w & P\tilde{B}_u \\ \tilde{B}_w^T P & 0 & 0 \\ \tilde{B}_u^T P & 0 & 0 \end{bmatrix}, \quad \Gamma_2 = \begin{bmatrix} \tilde{C}_z^T \\ \tilde{D}_{zw}^T \\ \tilde{D}_{zu}^T \end{bmatrix} M \begin{bmatrix} \tilde{C}_z & \tilde{D}_{zw} & \tilde{D}_{zu} \end{bmatrix}, \quad \Gamma_3 = \begin{bmatrix} \tilde{C}_y^T \\ \tilde{D}_{yw}^T \\ \tilde{D}_{yu}^T \end{bmatrix} \begin{bmatrix} \tilde{C}_y & \tilde{D}_{yw} & \tilde{D}_{yu} \end{bmatrix}, \quad \Gamma_4 = \begin{bmatrix} 0 & 0 & 0 \\ 0 & 0 & 0 \\ 0 & 0 & \beta^2 I \end{bmatrix}. \tag{25}$$

Now, if one restricts the first term in (24) to be positive (i.e., $[-\Gamma_1 - \lambda\Gamma_2 + \Gamma_3 - \Gamma_4] \succ 0$), then by neglecting the corresponding integral term, the following lower approximation is obtained:

$$||\mathcal{M}u||_{2T}^2 - \beta^2||u||_{2T}^2 \geq \int_0^T \begin{bmatrix} x \\ w \\ u \end{bmatrix}^T (\Gamma_1 + \lambda\Gamma_2) \begin{bmatrix} x \\ w \\ u \end{bmatrix} dt, \tag{26}$$

where the integral's value on the right-hand side is:

$$\int_0^T \begin{bmatrix} x \\ w \\ u \end{bmatrix}^T (\Gamma_1 + \lambda\Gamma_2) \begin{bmatrix} x \\ w \\ u \end{bmatrix} dt = -x^T(0)Px(0) - \lambda z^T(0)Mz(0). \tag{27}$$

Note that the latter is finite, therefore the system possesses a finite minimum gain by definition. At the same time, the technical condition on the positive definiteness of $-\Gamma_1 - \lambda\Gamma_2 + \Gamma_3 - \Gamma_4$ can be easily verified as the LMI condition of (20). ∎

Remark 1. The worst case induced $\mathcal{L}_2$ gain, $||\mathcal{M}||_{\Delta\infty} > \gamma$ can be calculated by replacing $\beta^2 I$ by $-\gamma^2 I$, and changing the sign of the last term (corresponding to $y^T y$) to + in (20). For more details we refer to Reference 2. Note that Reference 22 showed that this LMI condition can be satisfied by an indefinite $P \in \mathrm{S}^{n_x}$ as well.

Remark 2. Various uncertainties may be present in the system, with Δ having a blockdiagonal structure $\Delta = \mathrm{diag}\{\Delta_1, \ldots, \Delta_N\}$. Furthermore the (Ψ, M) IQC factorizations, serve as basis functions to describe each block in Δ. In a general case a blockdiagonal element in Δ may be best described by a linear combination of these basis functions, that is, the Δ_N term is characterized by the $\{(\Psi_{N1}, M_{N1}), \ \ldots \ (\Psi_{NR}, M_{NR})\}$ basis function set. As Reference 2 discusses, the presented method allows the treatment of several uncertainties in the analysis problem by replacing the corresponding term by

$$\sum_{n=1}^{N}\sum_{r=1}^{R} \lambda_{nr} \begin{bmatrix} \tilde{C}_{z_{nr}}^T \\ \tilde{D}_{zw_{nr}}^T \\ \tilde{D}_{zu_{nr}}^T \end{bmatrix} M_{nr} \begin{bmatrix} \star \end{bmatrix}, \tag{28}$$

with $\lambda_{nr} \geq 0$. The outer summation corresponds to the $[\Delta_1, \ \ldots, \ \Delta_N]$ blocks in Δ, while the inner one belongs to the $\{(\Psi_{N1}, M_{N1}), \ \ldots \ (\Psi_{NR}, M_{NR})\}$ basis function set describing each uncertainty block. Note that R may be different for each element in Δ.

4.2 | Robust minimum gain over finite frequency range

So far we have been assuming that the interconnected system is bi-proper (possesses a direct feed-through term). However, it is possible to calculate the minimum gain for systems where this condition is not fulfilled by the aid of the Generalized Kalman-Yakubovich-Popov (GKYP) lemma.[23,24] In this case the minimum sensitivity is computed over a selected frequency range of interest. In Reference 25 it is shown that the sensitivity of a system can be investigated over a certain frequency range if the system is controllable and its input is such that $u \in \mathcal{L}_2$ and the

$$\int_0^\infty \left(-\dot{x}\dot{x}^T + i\tilde{\omega}x\dot{x}^T - i\tilde{\omega}\dot{x}x^T - \underline{\omega}\overline{\omega}xx^T\right) dt \geq 0, \tag{29}$$

integral holds, with $\tilde{\omega} = \frac{\underline{\omega}+\overline{\omega}}{2}$. The following theorem extends Theorem 1 for systems without direct feed-through:

Theorem 2. *The robust minimum gain over a finite frequency domain. Assume that $\mathcal{F}_u(\mathcal{M}, \Delta)$ is well posed for all $\Delta \in$ IQC(Ψ, M). Let $\underline{\omega}$, $\overline{\omega}$ denote the minimum and maximum frequencies respectively in the interested frequency range, with $\tilde{\omega} = \frac{\underline{\omega}+\overline{\omega}}{2}$. Then $||\mathcal{F}_u(\mathcal{M}, \Delta)||_{\Delta-} > \beta$ if there exists a Hermitian P, Q and real $\lambda > 0$ such that $Q \succ 0$ and*

$$\begin{bmatrix} \tilde{A} & \tilde{B}_w & \tilde{B}_u \\ 0 & 0 & 0 \\ I & 0 & 0 \end{bmatrix}^T \Xi \begin{bmatrix} \star \end{bmatrix} + \begin{bmatrix} 0 & 0 & 0 \\ 0 & 0 & 0 \\ 0 & 0 & \beta^2 I \end{bmatrix} + \lambda \begin{bmatrix} \tilde{C}_z^T \\ \tilde{D}_{zw}^T \\ \tilde{D}_{zu}^T \end{bmatrix} M \begin{bmatrix} \star \end{bmatrix} - \begin{bmatrix} \tilde{C}_y^T \\ \tilde{D}_{yw}^T \\ \tilde{D}_{yu}^T \end{bmatrix} \begin{bmatrix} \star \end{bmatrix} \prec 0, \tag{30}$$

where $\Xi = \begin{bmatrix} \Phi_{11}Q & 0 & P + \Phi_{12}Q \\ 0 & 0 & 0 \\ P + \Phi_{21}Q & 0 & \Phi_{22}Q \end{bmatrix}$, *with* $\Phi = \begin{bmatrix} -1 & j\tilde{\omega} \\ -j\tilde{\omega} & -\underline{\omega}\overline{\omega} \end{bmatrix}$.

Proof. Multiplying the inequality in (30) by $\begin{bmatrix} x^T & w^T & u^T \end{bmatrix}$ from the left and by $\begin{bmatrix} x^T & w^T & u^T \end{bmatrix}^T$ from the right and then using the state space equations of (19), the following is derived:

$$\frac{d}{dt}(x^T P x) + \beta^2 u^T u + \lambda z^T M z - y^T y + \Phi_{11}\dot{x}^T Q \dot{x} + \Phi_{12}\dot{x}^T Q x + \Phi_{21} x^T Q \dot{x} + \Phi_{22} x^T Q x < 0. \tag{31}$$

This can be integrated along the state trajectory from $t = 0$ to $t = T$ to get:

$$\begin{aligned} &- x(0)^T P x(0) + \beta^2 \int_0^T u(t)^T u(t) dt + \lambda \int_0^T z(t)^T M z(t) dt - \int_0^T y^T(t) y(t) dt \\ &+ \int_0^T \left(\Phi_{11}\dot{x}^T Q \dot{x} + \Phi_{12}\dot{x}^T Q x + \Phi_{21} x^T Q \dot{x} + \Phi_{22} x^T Q x \right) dt < 0, \end{aligned} \tag{32}$$

where we have exploited the fact that $x \in \mathcal{L}_{2e}$. Then it follows from the IQC condition (11) that

$$\begin{aligned} &- x(0)^T P x(0) - \lambda z(0)^T M z(0) + \beta^2 \int_0^T u(t)^T u(t) dt - \int_0^T y^T(t) y(t) dt \\ &+ \operatorname{tr}\left[Q \textstyle\int_0^T \left(\Phi_{11}\dot{x}^T \dot{x} + \Phi_{12}\dot{x}^T x + \Phi_{21} x^T \dot{x} + \Phi_{22} x^T x \right) dt \right] < 0. \end{aligned} \tag{33}$$

Since $Q \succ 0$ and u satisfies condition (29) the tr[·] term is non-negative. Therefore we have

$$- x(0)^T P x(0) - \lambda z^T(0) M z(0) < \int_0^T y^T(t) y(t) dt - \beta^2 \int_0^T u(t)^T u(t) dt, \tag{34}$$

which completes the proof. ∎

5 | THE PROPOSED DECOUPLING ALGORITHM

Based on the derived minimum sensitivity conditions, we are now discussing the solution to the proposed RDP in Section 2. Our starting point is the $\mathcal{F}_u(\mathcal{M}, \Delta)$ interconnection of the known dynamics $\mathcal{M}$ and the uncertainty Δ, as shown in Figure 2.

Suppose that $\mathcal{M}$ is brought to a subsystem form, with $\mathcal{M} = \mathcal{M}_c + \mathcal{M}_d$ and state space matrices as:

$$A = \begin{bmatrix} A_c & 0 \\ 0 & A_d \end{bmatrix}, \quad B = \begin{bmatrix} B_{cw} & B_{cu} \\ B_{dw} & B_{du} \end{bmatrix}, \quad C = \begin{bmatrix} C_{cv} & C_{dv} \\ C_{cy} & C_{dy} \end{bmatrix}, \quad D = \begin{bmatrix} D_{vw} & D_{vu} \\ D_{yw} & D_{yu} \end{bmatrix}. \tag{35}$$

As it has been emphasized in Section 2 our aim is to find k_u and k_y transformation vectors which are minimizing the coupling, which appears only through the input- and output channels of the system. The remainder of the section is devoted to the calculation of these transformation vectors. This can be achieved in two consecutive steps. First an optimal input blend is found, and applied to the system, next a corresponding output blend is calculated.

Remark 3. Note that $\mathcal{M}$ may contain the dynamics of the nominal subsystems, and the weighting filters which are used to describe the frequency wise distribution of the uncertainties.

Remark 4. In the remainder of the section we will use $\mathcal{F}_u(\mathcal{M}_c, \Delta_c)$ and $\mathcal{F}_u(\mathcal{M}_d, \Delta_d)$ to describe well-posed uncertain subsystems. The subscripts at Δ are necessary in order to indicate different uncertainties in the various subsystems. As an example: an uncertain element in A_d will only affect $\mathcal{M}_d$, and not appear in Δ_c. Shared uncertainties (Δ_s) affecting both subsystems appear in Δ_c and Δ_d as well. However note that if there are uncertainties affecting both subsystems, then $\mathcal{F}_u(\mathcal{M}, \Delta) \neq \mathcal{F}_u(\mathcal{M}_c, \Delta_c) + \mathcal{F}_u(\mathcal{M}_d, \Delta_d)$. In this case the decomposition may lead to the removal of certain couplings between the subsystems through the shared elements in the Δ block. A possible (although conservative) remedy can be the selection of the (Ψ_i, M_i) IQC filters based on $\mathcal{F}_u(\mathcal{M}, \Delta)$, describing the $w_i = \Delta_i v_i$ relationship, and so constraining $w_i \in \mathcal{W}_i$, $v_i \in \mathcal{V}_i$ signals to belong the corresponding sets. Then, during the decoupling design, the same filters are applied for each subsystems to characterize the external signals. This approach restricts the signals corresponding to Δ_s to belong to the same set as in the $\mathcal{F}_u(\mathcal{M}, \Delta)$ case.

5.1 | Input blend calculation

In this subsection the computation of the input blend vector k_u is carried out, which maximizes the excitation of the targeted subsystem, while minimizes the impact on the one(s) to be decoupled. In Reference 1 it was shown that the LMI-based computation of the minimum sensitivity is only solvable for tall or square systems. This necessitates the application of an initial output blend[§] $k_{y0} \in \mathbb{R}^{1 \times n_y}$ to the system, which will assure that the upcoming design LMIs are written for tall systems.

The subsystems extended by the IQC filters are denoted by $\widetilde{\mathcal{M}}_c$ and $\widetilde{\mathcal{M}}_d$ respectively, with state space representations (with $i \in \{c, d\}$)

$$\begin{aligned} \dot{\tilde{x}}_{\{i\}} &= \tilde{A}_{\{i\}}\tilde{x}_{\{i\}} + \tilde{B}_{w,\{i\}}w + \tilde{B}_{u,\{i\}}u, \\ \tilde{z}_{\{i\}} &= \tilde{C}_{z,\{i\}}\tilde{x}_{\{i\}} + \tilde{D}_{zw}w + \tilde{D}_{zu}u, \\ y_{\{i\}} &= \tilde{C}_{y,\{i\}}\tilde{x}_{\{i\}} + \tilde{D}_{yw}w + \tilde{D}_{yu}u. \end{aligned} \tag{36}$$

The extended states are given by $\tilde{x}_{\{i\}} = \begin{bmatrix} x_i^T & x_{\Psi,\{i\}}^T \end{bmatrix}^T$, where $x_{\Psi,\{i\}}$ denotes the states of the IQC basis functions.

The layout for the input blend calculation is given in Figure 6: the upper subfigure[¶] shows the core of the concept, while the lower one represents the structure that is applied for the computations (discussed later). According to the problem formulation, the aim is to maximize the transfer from the single input signal $\underline{u}$ to the single output of the controlled subsystem $\underline{y}_c$, while at the same time minimize this transfer to the single output of the decoupled subsystem $\underline{y}_d$. In order to satisfy these goals, an n_u dimensional input blend vector k_u is introduced, which distributes the scalar $\underline{u}$ input between the real physical inputs of the system. Using our terminology the decoupling is formulated as: the

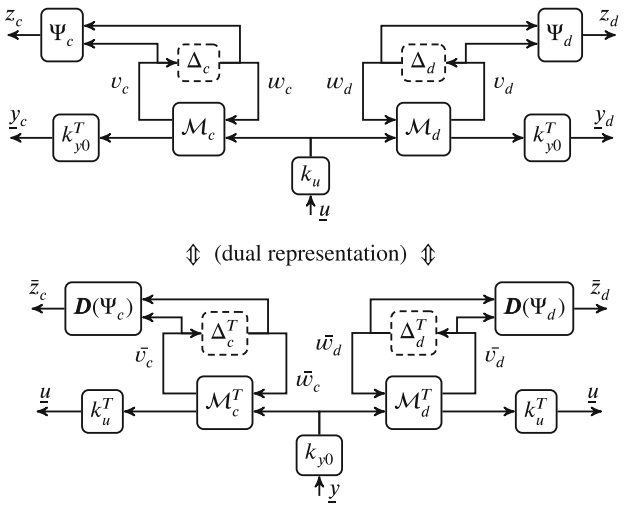

FIGURE 6 Problem layout for input blend calculation

minimum sensitivity from $\underline{u}$ to the performance output $\underline{y}_c$ is to be maximized, while the maximum sensitivity from $\underline{u}$ to $\underline{y}_d$ is minimized.

At this point it would be straightforward to put together all the building blocks by applying the systems' description (36) and the definition and computation of the minimum and maximum sensitivities (30), (A1) respectively. However, this would lead to a bi-linear optimization problem as shown in Reference 1. Therefore, the dual representation is applied, which preserves the input–output gain of a system, but facilitates linearity in the optimization variables. Accordingly, the dual IQCs $\boldsymbol{D}(\hat{\Psi})$ are used and the problem is reformulated as shown on the lower subfigure of Figure 6. By substituting $\mathcal{F}_u(\widetilde{\mathcal{M}}_c^T, \boldsymbol{D}(\hat{\Psi}_c))$ into (30), and introducing the new variable $K_u = k_u k_u^T$, the following form can be derived for the computation of the controlled subsystem's minimum gain:

$$\begin{bmatrix} \tilde{A}_c^T & \tilde{C}_{z,c}^T & \tilde{C}_{y,c}^T k_{y0} \\ 0 & 0 & 0 \\ I & 0 & 0 \end{bmatrix}^T \Xi \left[\star\right] + \begin{bmatrix} 0 & 0 & 0 \\ 0 & 0 & 0 \\ 0 & 0 & \beta^2 I \end{bmatrix} + \lambda_c \begin{bmatrix} \tilde{B}_{w,c} \\ \tilde{D}_{zw,c} \\ k_{y0}^T \tilde{D}_{yw,c} \end{bmatrix} M_c \left[\star\right] - \begin{bmatrix} \tilde{B}_{u,c} \\ \tilde{D}_{zu,c} \\ k_{y0}^T \tilde{D}_{yu,c} \end{bmatrix} K_u \left[\star\right] \prec 0, \tag{37}$$

where Ξ is given in (30). Similarly, by substituting $\mathcal{F}_u(\widetilde{\mathcal{M}}_d^T, \boldsymbol{D}(\hat{\Psi}_d))$ into (A1), the computation of the maximum gain of the subsystem is written as:

$$\begin{bmatrix} \tilde{A}_d^T P_d + P_d \tilde{A}_d & P\tilde{C}_{z,d}^T & P\tilde{C}_{y,d}^T k_{y0} \\ \star & 0 & 0 \\ \star & 0 & -\gamma^2 I \end{bmatrix} + \lambda_d \begin{bmatrix} \tilde{B}_{w,d} \\ \tilde{D}_{zw,d} \\ k_{y0}^T \tilde{D}_{yw,d} \end{bmatrix} M_d \left[\star\right] + \begin{bmatrix} \tilde{B}_{u,d} \\ \tilde{D}_{zu,d} \\ k_{y0}^T \tilde{D}_{yu,d} \end{bmatrix} K_u \left[\star\right] \prec 0. \tag{38}$$

These are the synthesis inequalities for finding the input blend vectors. Note that these inequalities are only linear because of the dual representation and the introduction of the $K_u = k_u k_u^T$ blend matrix variable, which is a dyadic product of the input blend vectors, that is, the newly introduced variable K_u is a rank 1 matrix, which has to be taken into consideration in the solution. Furthermore, inequality (37) and (38), are coupled through the same K_u variable, otherwise independent. The input blend calculation is summarized in Proposition 1.

Proposition 1. *The input blend design. The optimal robust input blend k_u for the system given in the form of $\mathcal{F}_u(\mathcal{M}, \Delta)$ can be calculated as the left singular vector corresponding to the largest singular value of the blend matrix K_u, where K_u satisfies the following optimization problem*

$$\begin{aligned} &\underset{P_d,\ \lambda_d,\ K_u,\ P_c,\ \lambda_c,\ Q_c,\ \beta^2,\ \gamma^2}{\text{minimize}} \quad -\beta^2 + \gamma^2 \\ &\text{subject to (37), (38),} \\ &P_d = P_d^T,\ P_d \succcurlyeq 0, \\ &P_c = P_c^T,\ Q_c = Q_c^T,\ Q_c \succcurlyeq 0, \\ &\lambda_c > 0,\ \lambda_d > 0, \\ &0 \preccurlyeq K_u \preccurlyeq I,\ \text{and rank}\,(K_u) = 1, \end{aligned} \tag{39}$$

with I being the identity matrix with appropriate dimensions.

Proposition 1 is a multi-objective optimization problem, which is frequent in mixed $\mathcal{H}_-/\mathcal{H}_\infty$ fault detection observer design (see e.g., Reference 20). More precisely, the two competing objectives (i.e., maximization of β^2 and minimization of γ^2) are merged into a single value by using scalarization. The proposed objective function can be considered as a special case of weighted scalarization, with weights equaling one. This expresses that no *apriori* knowledge is available before the optimization, however it can be changed in a later stage of the decoupling design. Furthermore, the proposed multi-objective optimization has a simple, but illustrative game-theoretic interpretation, where the two players wishes to reach their individual goals of maximizing β or minimizing γ together.[27] Since the two optimizations are connected through the shared variable K_u, the game is cooperative. It is known that the solution is then Pareto-optimal, that is, any decrease in one objective simultaneously increases the other one. In order to investigate this trade-off more systematically, the ϵ-constrained reformulation of (39) is invoked as follows

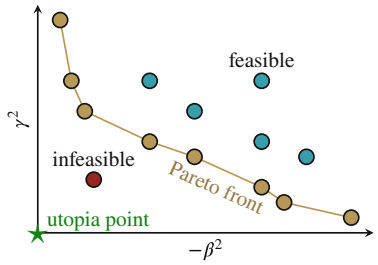

FIGURE 7 Pareto optimality

$$
\begin{aligned}
&\underset{P_d,\ \lambda_d,\ K_u,\ P_c,\ \lambda_c,\ Q_c,\ \beta^2,\ \gamma^2}{\text{minimize}} \quad -\beta^2 \\
&\text{subject to (37), (38),} \\
&\gamma^2 < \epsilon, \\
&P_d = P_d^T,\ P_d \succcurlyeq 0, \\
&P_c = P_c^T,\ Q_c = Q_c^T,\ Q_c \succcurlyeq 0, \\
&\lambda_c > 0,\ \lambda_d > 0, \\
&0 \preccurlyeq K_u \preccurlyeq I,\ \text{and rank}\,(K_u) = 1.
\end{aligned} \tag{40}
$$

In (40) the objective function is selected as one of the competing goals[#], while the other objective is constrained by a suitable chosen constant ϵ. By systematically varying ϵ the entire set of Pareto-optimal solutions can be generated.[28] This is illustrated in Figure 7, where the two objectives to be minimized are given in the x and y axis of the plot. The green star denotes an utopia point, where both objectives are minimal, but cannot be reached due to the trade-off between these goals. The Pareto-optimal solutions form the so-called Pareto-front, expressing that any decrease in one objective increases the other one. These are also called as Pareto-efficient solutions, to distinguish from other feasible points, where both objectives could be further decreased. The set of infeasible points cannot be reached due to the constraints. Finally we mention that the ϵ-constrained formulation of the decoupling can also be used for generating problem specific solutions with prescribed level of suppression (or excitation) by setting the ϵ value accordingly. Such solutions can be also achieved by changing the weights of the objectives in (39). However the user should keep in mind the trade-off, represented by the Pareto-front: minimizing the maximum sensitivity of the subsystem to be decoupled will also decrease the sensitivity of the targeted subsystem and vice versa.

As stated in (39), the optimization variable K_u has to be a rank-one solution, representing a non-convex constraint. This issue is addressed by adopting an alternating projection scheme, similarly to the nominal decoupling reported in Reference 1. Technical details are summarized in Appendix B, while for a more in-depth review please follow References 1 and 29.

Now we are in the position to present the solution to Proposition 1. Here-under we discuss its numerical steps, while the complete algorithm is given in Appendix C,

1. The solution process starts with defining the subsystem one wishes to control and the subsystem one wishes to decouple from it, that is, the system is transformed to the form given in the lower subfigure of Figure 6. This is the starting point of Algorithm 1, in line Algorithm 1.
2. Next the optimization problem presented in Proposition 1 is solved, without the arising rank constraint on K_u; the blend matrix is constrained to be symmetric and $0 \preccurlyeq K_u \preccurlyeq I$. This provides K_{u_0} which is then treated as the initial value in the following alternating projection sequence. The corresponding step is given in line 2 of Algorithm 1 and provides the achievable values for β and γ.
3. In the step of alternating projections (line 3) the computed β and γ are kept constant. Here, the inner loop iterations contain a series of alternating projections in order to obtain the corresponding reduced rank solution. Upon convergence, measured by a suitable metric, the outer loop reduces the rank further, until 1 is achieved. This optimal 1-rank solution is denoted by $K_u^\star$.
4. The blend vector k_u can be found from the singular value decomposition of the blend matrix $K_u^\star$: it is the left singular vector corresponding to the largest singular value of $K_u^\star$. Once k_u is computed, it is then applied to the input of the subsystems in (36) to obtain a single blended input description, forming the basis of the output blend calculation.

5.2 | Output blend calculation

After the optimal input blend is computed, a similar procedure can be carried out for determining a linear combination of the available outputs, such that the state information regarding the targeted subsystem is maximized, while it is minimized for the other subsystem. This is discussed briefly in this section. Using our notations k_y^T should create a single blended output, with having maximal sensitivity on the performance output of the subsystem to be controlled, and minimal transfer on the one to be decoupled. The approach is outlined in Figure 8.

The computation is essentially the same as for the input blend part, with the following modified LMI constraints:

$$\begin{bmatrix} \tilde{A}_c & \tilde{B}_{w,c} & \tilde{B}_{u,c}k_u \\ 0 & 0 & 0 \\ I & 0 & 0 \end{bmatrix}^T \Xi \left[\star\right] + \begin{bmatrix} 0 & 0 & 0 \\ 0 & 0 & 0 \\ 0 & 0 & \beta^2 I \end{bmatrix} + \lambda_c \begin{bmatrix} \tilde{C}_{z,c}^T \\ \tilde{D}_{zw,c}^T \\ k_u^T \tilde{D}_{zu,c}^T \end{bmatrix} M_c \left[\star\right] - \begin{bmatrix} \tilde{C}_{y,c}^T \\ \tilde{D}_{yw,c}^T \\ k_u^T \tilde{D}_{yu,c}^T \end{bmatrix} K_y \left[\star\right] \prec 0, \tag{41}$$

$$\begin{bmatrix} P_d\tilde{A}_d + \tilde{A}_d^T P_d & P_d\tilde{B}_{w,d} & P_d\tilde{B}_{u,d}k_u \\ \tilde{B}_{w,d}^T P_d & 0 & 0 \\ k_u^T \tilde{B}_{u,d}^T P_d & 0 & -\gamma^2 I \end{bmatrix} + \lambda_d \begin{bmatrix} \tilde{C}_{z,d}^T \\ \tilde{D}_{zw,d}^T \\ k_u^T \tilde{D}_{zu,d}^T \end{bmatrix} M_d \left[\star\right] + \begin{bmatrix} \tilde{C}_{y,d}^T \\ \tilde{D}_{yw,d}^T \\ k_u^T \tilde{D}_{yu,d}^T \end{bmatrix} K_y \left[\star\right] \prec 0. \tag{42}$$

The LMI condition (41) assures that the transfer through the controlled subsystem is maximized (with Ξ is given in (30)), and the satisfaction of (42) guarantees that the maximum sensitivity of the undesired dynamics is minimized. Note that, we have again introduced the new matrix variable $K_y = k_y k_y^T$. The optimization problem to be solved is given in Proposition 2 with variables P_c, Q_c, P_d, K_y, β^2, γ^2, λ_c, λ_d.

Proposition 2. *The output blend design. The optimal output blend vector k_y for the system with k_u input blend can be calculated as the left singular vector corresponding to the largest singular value of the blend matrix K_y, where K_y satisfies the following optimization problem*

$$\begin{aligned} &\underset{P_d,\ \lambda_d,\ K_y,\ P_c,\ \lambda_c,\ Q_c,\ \beta^2,\ \gamma^2}{\text{minimize}} \quad -\beta^2 + \gamma^2 \\ &\text{subject to (37), (38),} \\ &P_d = P_d^T,\ P_d \succcurlyeq 0, \\ &P_c = P_c^T,\ Q_c = Q_c^T,\ Q_c \succcurlyeq 0, \\ &\lambda_d > 0,\ \lambda_c > 0, \\ &K_y = K_y^T,\ 0 \preccurlyeq K_y \preccurlyeq I, \text{and rank}\left(K_y\right) = 1. \end{aligned} \tag{43}$$

The rank one solution for the blend matrix K_y is achieved again by applying the alternating projection scheme as for the input blend. The solution of Proposition 2 for the output blend vector k_y is a straightforward modification of the input blend calculation algorithm, by applying k_u as initial blend vector, and replacing (37), (38) by (41), (42).

Remark 5. In order to simplify the notations in (37), (38) and (41), (42), inequalities are given for a single block in Δ, described by a single $(\Psi,\ M)$ IQC. If multiple uncertainties are present, then we refer to Remark 2 to replace the corresponding terms in the inequalities.

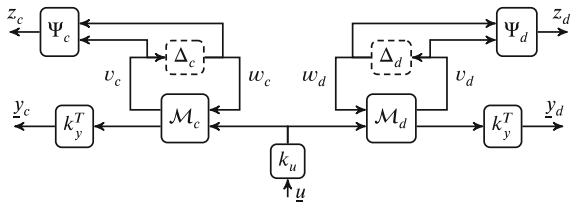

FIGURE 8 Problem layout for output blend calculation

Until this point we have considered the k_u and k_y input and output transformations as vectors. This is desirable because it significantly simplifies the control problem, by turning the plant into a SISO one. However these transformations may also be matrices, and sometimes this is necessary to achieve proper decoupling. In these cases there are 1 or more (n) singular values of K_{u0} which have comparable magnitude to the largest one. This means that there are n possible input directions which yield acceptable decoupling. On the contrary, the singular vectors corresponding to the smallest singular values of K_{u0} are denoting input directions which excite the decoupled dynamics. For keeping n input directions, one needs to run the alternating projection sequences $n_u - n$ times, where at the beginning of each sequences the smallest nonzero singular value of K_u is zeroed out (removing directions from K_u corresponding to the decoupled subsystem). For details see the alternating projection algorithm in Appendix B. Note that finding the desired value of n is problem dependent and may involve certain engineering judgment.

Note that the only assumptions we made so far are that the A matrix of $\mathcal{M}$ must have a blockdiagonal structure, or it has to be block-diagonalizable, and $\mathcal{F}_u(\mathcal{M}, \Delta)$ needs to be well posed. However some notes need to be taken about the case of unstable subsystems. The definition and analysis conditions provided in Section 4 for the robust minimum sensitivity also apply for unstable subsystems. The robust maximum sensitivity by definition applies for stable systems. In Reference 1 a workaround has been discussed by mirroring the unstable poles over the imaginary axis.

The application of input and output blends may introduce unstable zeros to the open loop SISO plant. Some of them are directly connected to the suppression of the undesired dynamics, and in the transfer function form may lead to pole-zero cancellations. On the other hand the appearance of additional zeros can be avoided when necessary by the fact that non-square systems rarely have transmission zeros.[5,30] This means that the open loop system might be converted to a non-square system by suitable input and (or) output transformation matrices.

Remark 6. The computation of the input and output blend vectors require an initial output and input blend vector, respectively. At the same time, the joint computation of the input and output blend calculations would lead to a bilinear optimization problem, whose solution is often obtained in an iterative manner with one variable fixed in each step. We suggest a similar computation for the k_u and k_y blend vectors. Starting from an initial k_{y0} an optimal solution for k_u is calculated based on Section 5.1 with a corresponding k_y relying on Section 5.2. Then by selecting $k_{y0} = k_y$ this iteration continues until convergence, defined by pre-set thresholds and the final values are then considered as optimal values. According to our numerical studies, better decoupling can be achieved through the iterative process than by separate design of the blend vectors. However in most cases the improvement provided by this iteration is marginal compared to the increased computational time, and so upon satisfactory results after the first step further iterations could be neglected.

6 | NUMERICAL EXAMPLES

This section provides numerical examples for evaluating the decoupling algorithm and for showing its effectiveness. First a simple academic example is given, which can be used for reproducing the results. Second, a more complex, real-world example is presented, where the flexible modes of an airplane are controlled, without interacting with the rigid body dynamics[‖].

6.1 | Academic example

In order to give an easily reproducible example, the following systems are considered.

$$\mathcal{G}_c = \left[\begin{array}{c|c} A_c & B_c \\ \hline C_c & D \end{array}\right] = \left[\begin{array}{ccc|ccc} -1.51 & -9.52 & 0 & 0.39 & 0.6 & 0.96 \\ 9.52 & -1.51 & 0 & 0.78 & 0.14 & 0 \\ 0 & 0 & p_c & 0 & -0.54 & -1.27 \\ \hline 1.6 & -0.39 & -1.56 & 0.61 & 1.51 & 1.27 \\ -1.04 & 0.66 & 0 & 0.91 & 1.29 & 0.21 \\ 0.39 & -0.36 & 0.81 & 1.61 & 1.38 & 1.66 \\ 2.12 & -0.26 & -0.55 & 1.02 & 1.17 & 0.82 \end{array}\right],$$

$$\mathcal{G}_d = \left[\begin{array}{ccc|ccc} -1.76 & 0 & 0 & -1.8 & -0.11 & -0.53 \\ 0 & -7.24 & 0 & -0.39 & -0.02 & 0 \\ 0 & 0 & p_d & 0.42 & -0.48 & 0.82 \\ \hline -0.56 & 0 & -0.76 & 0.61 & 1.51 & 1.27 \\ 0.94 & 0.19 & -0.58 & 0.91 & 1.29 & 0.21 \\ -1.79 & -0.68 & 0.61 & 1.61 & 1.38 & 1.66 \\ -0.51 & 0.37 & -0.32 & 1.02 & 1.17 & 0.82 \end{array}\right].$$

According to our terminology, $\mathcal{G}_c$ will play the role of the targeted subsystem, while $\mathcal{G}_d$ is the subsystem we wish to decouple. Both subsystems have 3 states, 3 inputs, and 4 outputs, and they are given in modal form with one uncertain parameter p_c and p_d respectively. These are treated as parametric uncertainties for characterizing uncertain pole locations. These parameters are assumed to be bounded as $p_c \in \left[-2.55, \quad -6.375\right]$ and $p_d \in \left[-1.272, \quad -4.2824\right]$. Thesystem is built up by these two subsystems as: $\mathcal{G}_p = \mathcal{G}_c + \mathcal{G}_d$.

One common source of uncertainties is unmodeled dynamics at higher frequencies, which is introduced in the example as a dynamic input multiplicative uncertainty. Accordingly, these blocks are appended to the system as $\mathcal{G}_u(s) = \mathcal{G}_p\left(I + W_m(s)\text{diag}\left(\Delta_1, \Delta_2, \Delta_2\right)\right)$, with SISO $||\Delta_{1,2}(s)|| \leq 1$ and

$$W_m(s) = \frac{s + 30.36}{1.25s + 101.2}. \tag{44}$$

This uncertainty description is common to cover neglected dynamics; where the specific form of W_m represents 30% uncertainty at low, and 80% uncertainty at high frequency ranges.[5]

Once the uncertainty channels are set up, the upper LFT representation of the uncertain system can be constructed as $\mathcal{F}_u(\mathcal{M}, \Delta)$, where $\Delta = \text{diag}(\Delta_1, \Delta_2, \Delta_2, \delta_c, \delta_d)$ with $||\Delta_{1,2}(s)|| \leq 1$, and $|\delta_{c,d}| \leq 1$. The latter being the reparametrized and normalized representations of the parameter uncertainties p_c and p_d. Note also that $\mathcal{F}_u(\mathcal{M}, \Delta)$ can be represented as the interconnection of two subsystems $\mathcal{F}_u(\mathcal{M}_c, \Delta_c)$ and $\mathcal{F}_u(\mathcal{M}_d, \Delta_d)$ respectively, with $\Delta_{c,d} = \text{diag}(\Delta_1, \Delta_2, \Delta_2, \delta_{c,d})$.

As discussed, in the IQC framework specific multipliers describe the behavior of each uncertainty block, so, the next question is the appropriate filter selection. $\Delta_{1,2}$ are dynamic SISO LTI uncertainties, with $||\Delta_{1,2}(s)|| < 1$, and for this case Reference 17 proposes an IQC multiplier in the form of

$$\Pi_\Delta(j\omega) = \begin{bmatrix} x(j\omega)I & 0 \\ 0 & -x(j\omega)I) \end{bmatrix}, \tag{45}$$

where $x(j\omega) > 0$ is a stable, measurable function. Due to the special and simple form of (45) the $(\Psi,\ M)$ pair can be directly selected by picking

$$M_\Delta = \begin{bmatrix} 1 & 0 \\ 0 & -1 \end{bmatrix}, \quad \Psi_\Delta(s) = \begin{bmatrix} \frac{s+106}{s+9.639} & 0 \\ 0 & \frac{s+106}{s+9.639} \end{bmatrix}. \tag{46}$$

The numerical values of $\Psi_\Delta(s)$ were selected such that it gives an upper bound on the maximum singular value curves of the sampled uncertain subsystems, and has a slightly higher natural frequency than those. According to the uncertainty modeling formalism, three separate $\Psi_\Delta(s)$ filters are connected to the input–output channels of the Δ block corresponding to each $\Delta_{1,2}$ block respectively.

The uncertain pole locations are described by the $|\delta_i| \leq 1$ parametric uncertainties. The corresponding dynamic multiplier suggested by Megretski and Rantzer[17] has the form of

$$\Pi_\delta(j\omega) = \begin{bmatrix} X(j\omega) & Y(j\omega) \\ Y(j\omega)^* & -X(j\omega) \end{bmatrix}, \tag{47}$$

where $X(j\omega) = X(j\omega)^* \geq 0$ and $Y(j\omega) = -Y(j\omega)^*$ are bounded and measurable matrix functions. The SISO $X(j\omega)$ and $Y(j\omega)$ transfer functions were initially selected to over-bound the maximum singular value curves of the sampled uncertain

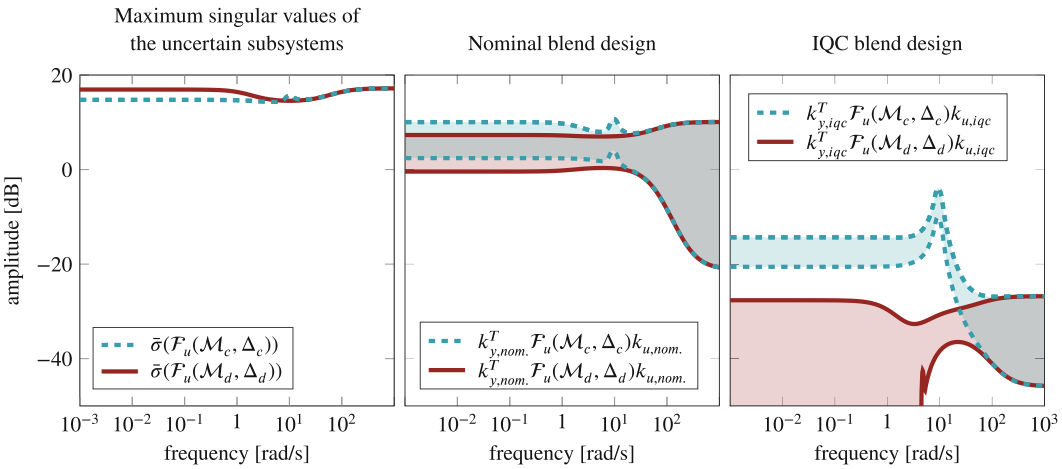

FIGURE 9 Academic example, subsystem decoupling results

subsystems, and then adjusted for better decoupling. A hard factorization of Π_δ is provided by its J-spectral factorization, as described in the appendix B of Reference 2. By selecting $\Pi_\delta(j\omega)$ as

$$\Pi_\delta(s) = \begin{bmatrix} \frac{96.39}{s+96.39} & \frac{s}{s+0.255} \\ \frac{s}{s-0.255} & \frac{-96.39}{s+96.39} \end{bmatrix}, \tag{48}$$

it's J-spectral factorization is:

$$J_\delta = \begin{bmatrix} 1 & 0 \\ 0 & -1 \end{bmatrix}, \quad \hat{\Psi}_\delta(s) = \begin{bmatrix} \frac{0.70711(s+198.4)}{s+96.39} & \frac{0.70711(s+47.02)}{(s+96.39)} \\ \frac{-70711(s+47.02)}{(s+96.39)} & \frac{0.70711(s+198.4)}{(s+96.39)} \end{bmatrix}. \tag{49}$$

In the example we want to achieve decoupling over the $[0, \quad \overline{\omega}]$ frequency range, where $\overline{\omega}$ was selected as the 10 times of the maximum natural frequency (96.4 rad/s) of the targeted subsystem $\mathcal{G}_c$. The dynamical models have been extended with the IQC descriptions and the corresponding algorithms were performed in order to calculate the input and output blend vectors.

Upon computing the blend vectors, the decoupling performance is evaluated in the frequency domain, based on the singular values of the blended subsystems, shown in Figure 9. Instead of specific singular value curves, shaded intervals are plotted denoting the ranges where the uncertain singular values may fall. Green and red colors correspond to the controlled and decoupled subsystems, respectively. Clearly our aim is to separate the two sets of curves by maximizing the difference between these ranges, and having higher gains through the controlled subsystem than through the one to be decoupled.

The left subfigure of Figure 9 shows the robust maximum gains of the subsystems over frequency, before applying the blend vectors. Note that without blending, the subsystems to be decoupled have higher amplifications through certain input–output pairs than the controlled ones. The results were calculated by MATLAB's *wcgain* function.

The middle subfigure of Figure 9 presents a nominal design based on the algorithm published in Reference 1. Here the corresponding input and output blend vectors have been computed based on a nominal model, with $p_c = -2.55$, $p_d = -4.24$ and neglecting the input multiplicative uncertainties. These blend vectors are then applied to the uncertain dynamics and visualized in the plot. As it can be depicted the nominal decoupling decreased the gap between the two sets of curves, however the two areas are overlapping. That is, the nominal vectors cannot guarantee robust decoupling, there might be cases when the decoupled subsystem has higher amplification than the controlled one. The upper bounds of the shaded areas were computed by MATLAB's *wcgain* function. Then by MATLAB's *usample* function samples were taken such that the uncertainties are uniformly distributed in their variation intervals. Then a frequency a wise lower bound was calculated as the minimum values of the corresponding sets at each frequency.

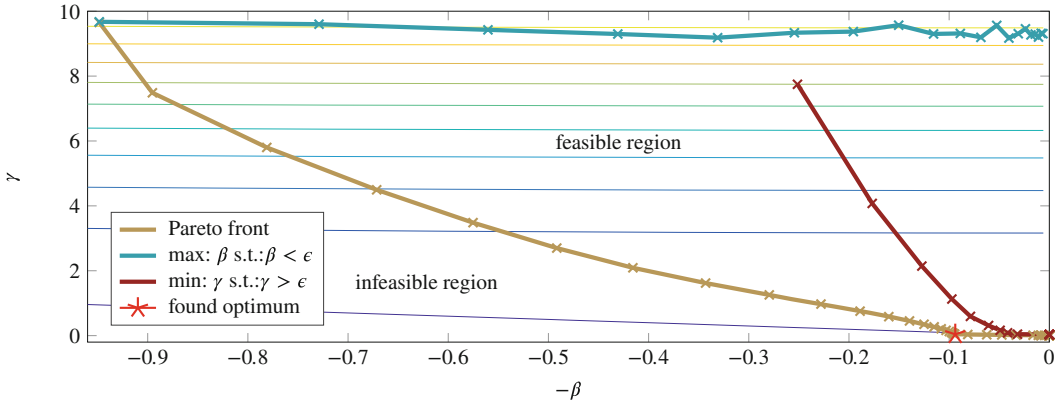

FIGURE 10 Pareto front for the output blend calculation of the academic example

The right subfigure of Figure 9 shows the robust design case. It is obvious that up to the maximum natural frequency (9.64 rad/s) of the targeted subsystem decoupling is achieved. The controlled subsystem's gains are higher than the one to be decoupled. At the same time, the sensitivity of the controlled subsystem has also been decreased, compared to the nominal design case, which is a price that one has to pay in order to achieve robust decoupling. The discussed game-theoretic interpretation of the solution has also been calculated for the academic example and summarized in Figure 10 for better understanding the trade-off. The yellow curve represents the Pareto-front computed by using the ϵ-constrained method as in (40) with different values of ϵ, these are the Pareto-efficient solutions. The blue and the red curves refer to the corresponding single objective optimization problems. In these optimization only one of the two objectives has been considered and solved for different values of ϵ, without any information about the "other" subsystem. The resulting blend matrices are then applied for the complementary subsystems to see the achieved effects. These are the solutions for the non-cooperative games, where the two players are aiming to minimize their respective costs only.[28] It can be depicted that β maximization can achieve a high minimum sensitivity (≈ 0.95), however the corresponding γ value is also high (≈ 10). On the other hand, minimizing only γ can lead to small values, but the resulting blend matrix also decreases the β significantly. Lastly, the solution to the optimization in (39) is denoted by the red star. To evaluate this result, the contour plots of the scalarized objective function $-\beta^2 + \gamma^2$ are also given in Figure 10. Along each line, the cost is constant, while they increase from the bottom to the top. Accordingly, one can depict that the red star has actually the minimal cost with the highest β value among the Pareto-efficient solutions.

In order to test the dependency of the blend vectors on the initial conditions, a numerical convergence analysis has been carried out. By setting randomized initial conditions k_{u0} and k_{y0} for the input and output blend calculations, with $|k_{u0}|_2 = 1$ and $|k_{y0}|_2 = 1$, the k_u and k_y vectors were recalculated 100 times. These results showed that after the iteration is converged the recalculated k_u and k_y blend vectors pointed in the same direction as the original ones used in the article. Note that in this case the blend calculation steps given in Sections 5.1 and 5.2 did not depend on each other.

6.2 | Aerospace example

The next example shows a possible application of the robust decoupling, based on a flexible wing aircraft model[31] developed in the FLIPASED project.[32] This UAV airplane serves as a testbed for investigating various flutter suppression techniques. Flutter is a phenomena which originates from the interaction of the aerodynamic- and structural forces, leading to a lightly damped or unstable oscillating motion of the wings. If this oscillation is not suppressed properly it might lead to premature material fatigue endangering the structural integrity of the aircraft. In the example we aim to find input and output combinations which assure that the asymmetric flutter mode is decoupled from the rigid body dynamics, even if our knowledge of the plant is uncertain. The physical interpretation of this decoupling is straightforward: facilitating the separate design of a flutter suppression controller, without changing the rigid-body autopilot.

A nonlinear model of the flexible wing aircraft has been presented in Reference 31. For the purpose of this example, the nonlinear model has been linearized at the 50 m/s airspeed, yielding an LTI model with 12 inputs, 6 outputs, and 12 states. Eight states describe the usual rigid body aircraft dynamics, while the remaining 4 represents symmetric and asymmetric flutter modes corresponding to the flexible dynamics. The aircraft has 8 ailerons (4-4 on each wing) and a V-tail configuration accommodating 4 ruddervators (2-2 on each side). Opposite deflections of the ruddervators correspond to an elevator input, while deflections to the same direction create a rudder input. Measurements are carried out at both wing tips, and they include vertical accelerations, and angular rates about the x and y axis respectively. In the example three different types of uncertainties are considered.

1. Dynamic input multiplicative uncertainties are connected to the two inner ailerons describing the effects of unmodeled dynamics and the mismodeling of the actuators (only two were considered in order to avoid inflating the problem's dimension). Similarly to the previous example, 30% uncertainty is added to the low, and 80% is added to the high frequencies.
2. One common issue in the literature of flutter modeling and control, is the exact knowledge of the parameters of flexible modes.[33] In order to reflect this issue, a parametric uncertainty is introduced for the poles of the asymmetric flutter dynamics: the A_c matrix is multiplied by an uncertain parameter, introducing a $\pm 40\%$ variation. In addition, the poles of the roll subsidence and the spiral modes were allowed to vary by $\pm 10\%$.
3. Lastly 1-1 memoryless nonlinearities were connected to the outer two ailerons describing the fact that their effectiveness is not precisely modeled. These are treated as sector bounded nonlinearities over the sector $\begin{bmatrix} 0 & \zeta \end{bmatrix}$. Note that Δ_ζ belongs to this sector if

$$\Delta_\zeta(v,t)(\zeta v - \Delta_\zeta(v,t)) \geq 0, \tag{50}$$

holds for all $v, t \in \mathbb{R}$.[2] In our example $\zeta = 0.2$ was selected, which is then expressed by an IQC multiplier as

$$M_\zeta = \begin{bmatrix} 0 & \zeta \\ \zeta & -2 \end{bmatrix}, \quad \Psi_\zeta(s) = \begin{bmatrix} 1 & 0 \\ 0 & 1 \end{bmatrix}. \tag{51}$$

This is depicted in Figure 11, where the aircraft denotes the nominal model when the parametric uncertainties are pulled out by an LFT transformation to the corresponding Δ block. Similarly to the previous one, this example also evaluates the decoupling performance based on frequency domain responses. The decoupling problem is considered to be successful, when the controlled subsystem takes its values from a higher area on the singular value plot, than the decoupled one. The results are shown in Figure 12. The left subfigure shows the robust maximum gains corresponding to the two subsystems before applying the blend vectors. Note that without blending, the subsystems to be decoupled have higher amplifications through certain input–output pairs then the controlled ones. The remaining two

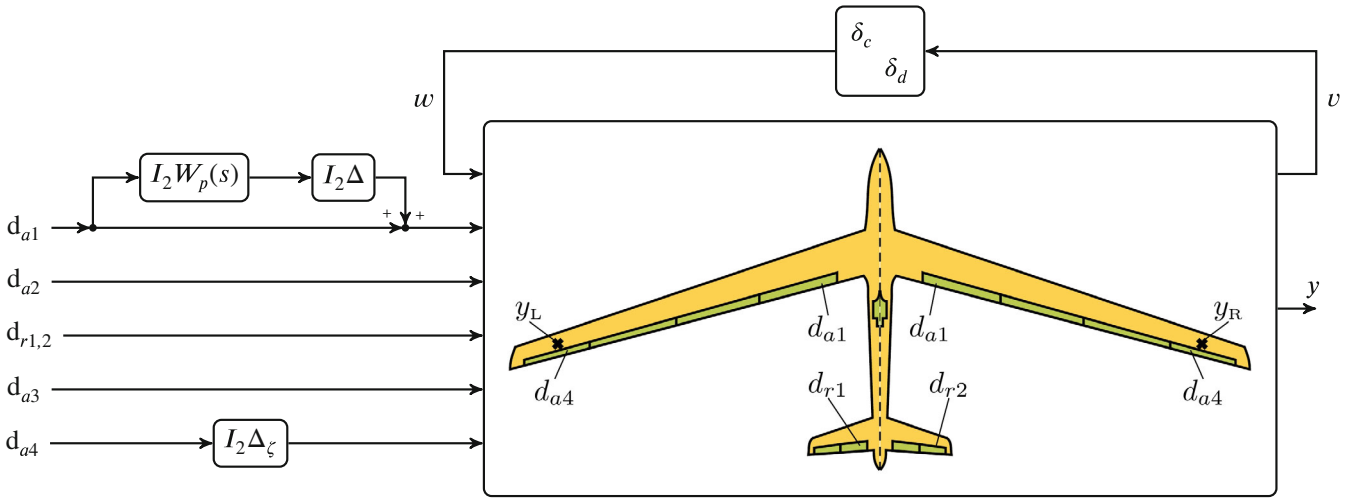

FIGURE 11 Aerospace example layout

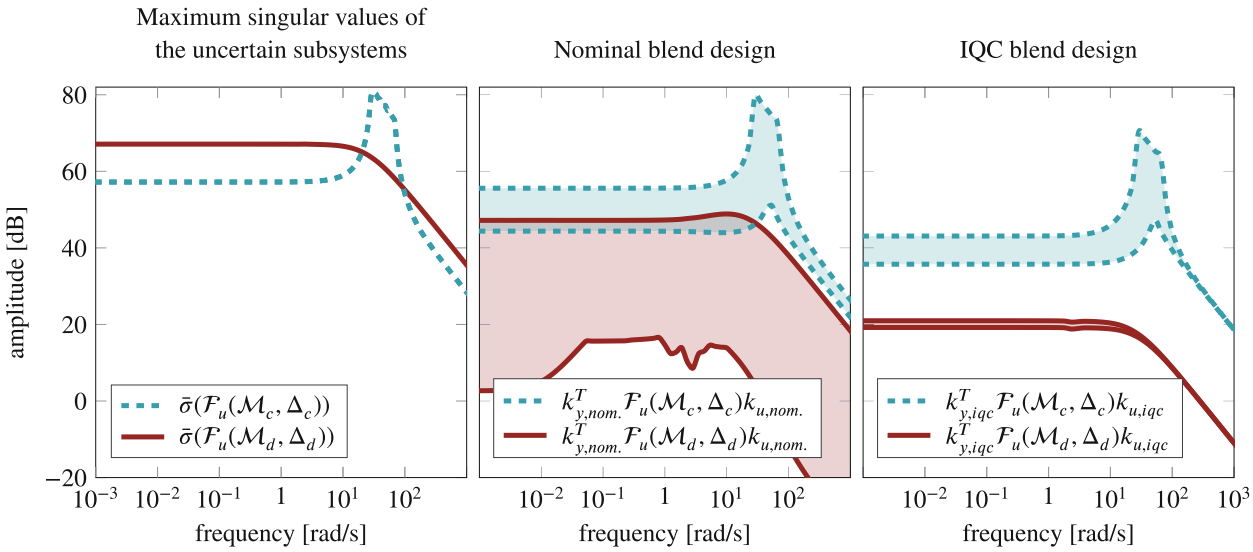

FIGURE 12 Aerospace example, subsystem decoupling results

subfigures show the transfer characteristics of the blended subsystems. The nominal blend vectors were designed for the subsystems without uncertainties. The middle subfigure shows that decoupling cannot be guaranteed in this case, because there might be an uncertainty combination, that the decoupled subsystem has higher gain than the flutter mode. However, if one is taking into account the underlying uncertainties, as discussed in the article, then it is possible to robustly decouple the subsystems. This is shown in the right subfigure of Figure 12. Note that the approximately 20 dB gap between the two areas represents that the controlled subsystem has a 10 times higher sensitivity than the other dynamics.

7 | CONCLUSIONS

The article proposed a robust decoupling scheme for LTI systems with LFT interconnected uncertainty, where the behavior of the uncertain blocks were assumed to be described by IQCs. First an LMI based analysis result is established for the computation of the robust minimum gain of such systems. Infinite and finite frequency ranges are treated separately, with different analysis conditions. Based on the derived results a robust decoupling scheme was proposed, where blend vectors are synthesized to maximize the excitation of the targeted subsystem, and attenuate the effects on the decoupled ones. Numerical algorithms are provided along with their applications. The reported examples clearly show that, the systematic handling of model uncertainties increases the robust decoupling performance.

Besides the work covered in the article, the authors are aware that there are several open questions to be answered in the future. Exact decoupling conditions, characterizing under what conditions is it possible to decouple the subsystems, are not yet established. There are several numerical issues that also have to be addressed in order to provide a solid framework for system's decoupling. This is mainly due to the fact that the conservativness of the IQC analysis conditions are sensitive to the applied filters. Although their are guidelines to how to select the structure of a filter, the precise description of the underlying uncertainty with minimal number of filters is still an open question. However, the achieved results are promising and the applied mathematical framework allows the extension of the method for linear parameter varying systems as well.

ACKNOWLEDGMENTS

The research leading to these results is part of the FLIPASED project. This project has received funding from the European Unions Horizon 2020 research and innovation programme under Grant agreement No. 815058. The research

was supported by the Ministry of Innovation and Technology NRDI Office within the framework of the Autonomous Systems National Laboratory Program. The authors thank Peter Seiler for his valuable comments on the manuscript. T. Luspay expresses his gratitude to Tsering Wangmo.

CONFLICT OF INTEREST

The authors have no conflict of interest to declare.

DATA AVAILABILITY STATEMENT

The data that support the findings of this study are available from the corresponding author upon reasonable request.

ENDNOTES

*Note that this special form describes the parallel interconnection of the underlying subsystems.

†The article only discusses the decoupling transformations. The underlying $C(s)$ controller can be designed by any robust control technique, and the calculated transformation vectors will assure that it does not interact with the decoupled dynamics.

‡The minimum sensitivity is evaluated over a specified $[\underline{\omega}, \overline{\omega}]$ frequency interval, ensuring a non-zero value for strictly proper systems.

§The initial k_{y0} output blend has to be selected such that it does not turn any of the subsystems unobservable. Note that selecting k_{y0} as a column of ones usually suffices. If not, initial k_{y0} can be found based on the Popov-Belevitch-Hautus (PBH) observability test.[26] It states that the system is observable if rank $\begin{bmatrix} k_{y0}^T C \\ sI - A \end{bmatrix} = n_x$. In other words for all p eigenvectors of A, the $k_{y0}^T Cp \neq 0$ relationship must hold. By collecting all eigenvectors to a P matrix, k_{y0} can be found as a solution to $k_{y0}^T CP = \mathbf{1}$, where $\mathbf{1}$ is a vector of ones with appropriate dimension. For complex eigenvalues the real and imaginary parts of a corresponding eigenvector have to be substituted.

¶Note that $\mathcal{M} = \mathcal{M}_c + \mathcal{M}_d$, from what it follows that the y_c and y_d output signals should also be added to formulate the output of $\mathcal{M}$. However since we are interested in the transfer properties of the individual subsystems, for brevity this addition is neglected in the figure.

#Alternatively the value of β can also be constrained while minimizing only γ.

‖The following numerical examples are relying on the hard IQC factorizations given by the $(\Psi,\ M)$ pair. In some case this factorization can be easily found (e.g., dynamic uncertainty), however in other cases the hard factorization needs to be calculated numerically for example by the J-spectral factorization (see Section 3.1). This leads to the $\left(\hat{\Psi},\ J\right)$ pair. While the analysis and synthesis inequalities were written for the $(\Psi,\ M)$ pair in the article, it should be obvious that $\left(\hat{\Psi},\ J\right)$ is used whenever it is available.

ORCID

Tamás Baár https://orcid.org/0000-0003-0036-4114
Tamás Luspay https://orcid.org/0000-0002-3845-576X

REFERENCES

1. Baár T, Luspay T. Decoupling through input-output blending. *Int J Control*. 2021;94(12):3491-3505.
2. Pfifer H, Seiler P. Robustness analysis of linear parameter varying systems using integral quadratic constraints. *Int J Robust Nonlinear Control*. 2015;25(15):2843-2864.
3. Bridgeman LJ, Forbes JR. The minimum gain lemma. *Int J Robust Nonlinear Control*. 2015;25(14):2515-2531.
4. Liu L, Tian S, Xue D, Zhang T, Chen Y, Zhang S. A review of industrial MIMO decoupling control. *Int J Control Autom Syst*. 2019;17(5):1246-1254.
5. Skogestad S, Postlethwaite I. *Multivariable Feedback Control: Analysis and Design*. 2. Wiley 2007.
6. Mohammadpour J, Grigoriadis K, Franchek M, Wang YY, Haskara I. LPV decoupling for control of multivariable systems. *Int J Control*. 2011;84(8):1350-1361.
7. Wang QG. *Decoupling Control*. Vol 285. Springer Science & Business Media; 2002.
8. Chakravarthy A, Deodhare G, Patel VV, Saraf A. Design of notch filters for structural responses with multiaxis coupling. *J Guid Control Dyn*. 1999;22(2):349-357.
9. Pitt D, Hayes B, Goodman C. F/A-18E/F aeroservoelastic design, analysis, and test. Proceedings of the 44th AIAA/ASME/ASCE/AHS/ASC Structures, Structural Dynamics, and Materials Conference; 2003:1880.
10. Theis J, Pfifer H, Seiler PJ. Robust control design for active flutter suppression. Proceedings of the AIAA Atmospheric Flight Mechanics Conference; 2016:1751.
11. Danowsky BP, Thompson P, Lee DC, Brenner MJ. Modal isolation and damping for adaptive aeroservoelastic suppression. Proceedings of the AIAA Atmospheric Flight Mechanics (AFM) Conference; 2013.
12. Pusch M. Aeroelastic mode control using H_2-optimal blends for inputs and outputs. Proceedings of the 2018 AIAA Guidance, Navigation, and Control Conference; 2018:618-630.
13. Pusch M, Ossmann D. H2-optimal blending of inputs and outputs for modal control. *IEEE Trans Control Syst Technol*. 2019;28(6):2744-2751.

14. Pusch M, Ossmann D, Dillinger J, Kier TM, Tang M, Lübker J. Aeroelastic modeling and control of an experimental flexible wing. Proceedings of the AIAA Scitech 2019 Forum; 2019:131-146.
15. Pusch M, Ossmann D, Luspay T. Structured control design for a highly flexible flutter demonstrator. *Aerospace*. 2019;6:27-47.
16. Baár T, Luspay T. Robust minimum gain lemma. Proceedings of the 2021 60th IEEE Conference on Decision and Control (CDC); 2021; IEEE.
17. Megretski A, Rantzer A. System analysis via integral quadratic constraints. *IEEE Trans Automat Contr*. 1997;42(6):819-830.
18. Seiler P. Stability analysis with dissipation inequalities and integral quadratic constraints. *IEEE Trans Automat Contr*. 2014;60(6):1704-1709.
19. Venkataraman R, Seiler P. Convex LPV synthesis of estimators and feedforwards using duality and integral quadratic constraints. *Int J Robust Nonlinear Control*. 2018;28(3):953-975.
20. Wang JL, Yang GH, Liu J. An LMI approach to H_- index and mixed H_-/H_∞ fault detection observer design. *Automatica*. 2007;43(9):1656-1665.
21. Glover K, Varga A. On solving non-standard $H_-/H_{2/\infty}$ fault detection problems. Proceedings of the 2011 50th IEEE Conference on Decision and Control and European Control Conference; 2011:891-896; IEEE.
22. Pfifer H, Seiler P. Less conservative robustness analysis of linear parameter varying systems using integral quadratic constraints. *Int J Robust Nonlinear Control*. 2016;26(16):3580-3594.
23. Wang H, Yang GH. A finite frequency domain approach to fault detection observer design for linear continuous-time systems. *Asian J Control*. 2008;10(5):559-568.
24. Iwasaki T, Hara S. Generalization of Kalman-Yakubovic-Popov lemma for restricted frequency inequalities. Proceedings of the 2003 American Control Conference; Vol. 5, 2003:3828-3833; IEEE.
25. Iwasaki T, Hara S, Fradkov AL. Time domain interpretations of frequency domain inequalities on (semi) finite ranges. *Syst Control Lett*. 2005;54(7):681-691.
26. Kailath T. Linear Systems. 156 Prentice-Hall 1980.
27. Marden JR, Shamma JS. Game theory and control. *Annu Rev Control Robot Auton Syst*. 2018;1:105-134.
28. Rao S. Game theory approach for multiobjective structural optimization. *Comput Struct*. 1987;25(1):119-127.
29. Grigoriadis KM, Beran EB. Alternating projection algorithms for linear matrix inequalities problems with rank constraints. *Advances in Linear Matrix Inequality Methods in Control*. SIAM; 2000:251-267.
30. Schrader CB, Sain MK. Research on system zeros: a survey. *Int J Control*. 1989;50(4):1407-1433.
31. Meddaikar YM, Dillinger J, Klimmek T, et al. Aircraft aeroservoelastic modelling of the flexop unmanned flying demonstrator. Proceedings of the AIAA Scitech 2019 Forum; 2019; AIAA.
32. FliPASED. Flight phase adaptive aero-servo-elastic aircraft design methods (FliPASED). Project of the European Union, Project ID: 815058; 2019-2022.
33. Danowsky BP, Schmidt DK, Pfifer H. Control-oriented system and parameter identification of a small flexible flying-wing aircraft. Proceedings of the AIAA Atmospheric Flight Mechanics Conference; 2017:1394.

How to cite this article: Baár T, Luspay T. Robust decoupling of uncertain subsystems. *Int J Robust Nonlinear Control*. 2022;32(10):6086-6109. doi: 10.1002/rnc.6141

APPENDIX A. WORST-CASE GAIN CALCULATION

The worst case gain can be calculated as follows. Append the Ψ filter to the LFT interconnection to get an extended system as shown in Figure 5. The dynamics of this interconnection is described by (19). Then the robust maximum sensitivity is given by the following lemma.

Lemma 3. *Robust maximum sensitivity.*[2] *Assume that $\mathcal{F}_u(\mathcal{M}, \Delta)$ is well posed for all $\Delta \in \mathrm{IQC}(\Psi, M)$, and the interconnection is stable. Then the worst-case gain is finite and less than γ, if there exists a $P \in \mathrm{S}^{n_x} \succ 0$ and $\lambda > 0$ such that*

$$\begin{bmatrix} PA + A^TP & PB_w & PB_u \\ B_w^TP & 0 & 0 \\ B_u^TP & 0 & -\gamma^2 I \end{bmatrix} + \lambda \begin{bmatrix} C_z^T \\ D_{zw}^T \\ D_{zu}^T \end{bmatrix} M \begin{bmatrix} \star \end{bmatrix} + \begin{bmatrix} C_y^T \\ D_{yw}^T \\ D_{yu}^T \end{bmatrix} \begin{bmatrix} \star \end{bmatrix} \prec 0, \tag{A1}$$

is satisfied.

Proof. The proof can be found in Reference 2. ∎

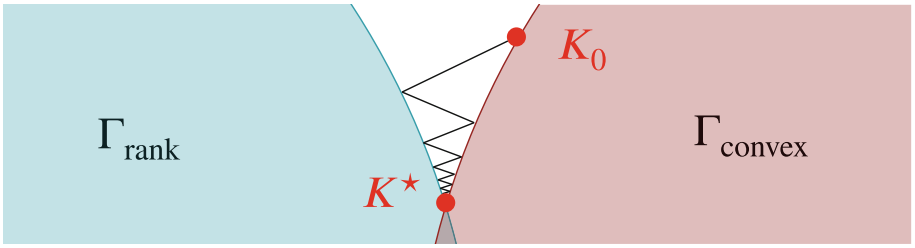

FIGURE B1 Alternating projections

APPENDIX B. ALTERNATING PROJECTIONS

Define two sets, with a possible intersection, as shown in Figure B1. The Γ_{convex} set is described by the LMIs (37) and (38). This is the solution set of Proposition 1, without the rank constraint. Γ_{rank} denotes the non-convex rank constraint on K_u. We are interested in finding a solution at the intersection of the two sets, denoted by $K_u^\star$ in Figure B1. The alternating projection algorithm has two consecutive steps in a sequence. The first step involves an orthogonal projection from the Γ_{convex} to the Γ_{rank} set by Lemma 4. This assures that the rank of K_u is reduced by 1. In a second step one needs to project this reduced rank K_u matrix back to the Γ_{convex} solution set. This is done based on Lemma 5. Then one needs to iterate these two steps until a solution is found in the intersection of the two sets. If a solution is found, then the rank of K_u has been successfully decreased by 1. In order to satisfy the rank constraint in Proposition 1, the whole projection sequence shown in Figure B1 has to be evaluated n_u-1 times until $\text{rank}(K_u^\star) = 1$ is achieved. Lemmas 4 and 5 are as follows.

Lemma 4. *Orthogonal projection to a lower dimensional set.*[29] *Let* $Z \in \Gamma_{\text{rank}}^{n\times n}$ *and let* $Z = USV^T$ *be a singular value decomposition of* Z. *The orthogonal projection,* $Z^\star = \mathcal{P}_{\Gamma_{\text{rank}}^{n-k}} Z$, *of* Z *onto the* $\Gamma_{\text{rank}}^{n-k\times n-k}$ *dimensional set is given by*

$$Z^\star = US_{n-k}V^T, \tag{B1}$$

where the S_{n-k} *diagonal matrix is obtained by replacing the smallest k singular values by zeros.*

Lemma 5. *Projection to a general LMI constraint set* Γ.[29] *Let* Γ *be a convex set, described by an LMI. Then the projection* $X^\star = P_\Gamma X$ *can be computed as the unique solution* Y *to the semidefinite programing problem*

$$\begin{aligned} &\text{minimize} \quad \text{trace}(S) \\ &\text{subject to} \begin{bmatrix} S & Y-X \\ Y-X & I \end{bmatrix} \geqslant 0, \\ &Y \in \Gamma,\ S, Y, X \in R^{n\times n}, \end{aligned} \tag{B2}$$

with $S = S^T$.

Proof. For further details about the projection sequences the reader is invited to consult with Reference 29. ∎

The alternating projection technique is an effective tool to find a $K^\star$ at the intersection of the Γ_{rank} and Γ_{convex} sets. However it does not guarantee global optimality of the solution, and the point of convergence heavily depends on the initial condition K_0. In some cases, especially when the intersecting angle between the two sets is small, the rate of convergence to a feasible solution at the intersection may degrade. In this case the directional alternating projection algorithm may provide faster convergence. For details see Reference 29.

APPENDIX C. THE INPUT BLEND CALCULATION ALGORITHM

Algorithm 1. Input blend calculation with alternating projection

Given: The subsystems $\mathcal{F}_u(\mathcal{M}_c, \Delta)$ and $\mathcal{F}_u(\mathcal{M}_d, \Delta)$ are given in a form as shown in Figure 6.

Initialization: Solve the following optimization problem, for β^2, γ^2, λ_c, λ_d, P_d, P_c, Q_c, K_u:

$$\underset{P_d,\, K_u,\, P_c,\, Q,\, \beta^2,\, \gamma^2,\, \lambda_c,\, \lambda_d}{\text{minimize}} \quad -\beta^2+\gamma^2$$

s.t.:

$$\begin{bmatrix} \tilde{A}_c^T & \tilde{C}_{z,c}^T & \tilde{C}_{y,c}^T k_{y0} \\ 0 & 0 & 0 \\ I & 0 & 0 \end{bmatrix}^T \Xi\left[\star\right] + \begin{bmatrix} 0 & 0 & 0 \\ 0 & 0 & 0 \\ 0 & 0 & \beta^2 I \end{bmatrix} + \lambda_c \begin{bmatrix} \tilde{B}_{w,c} \\ \tilde{D}_{zw,c} \\ k_{y0}^T \tilde{D}_{yw,c} \end{bmatrix} M_c\left[\star\right] - \begin{bmatrix} \tilde{B}_{u,c} \\ \tilde{D}_{zu,c} \\ k_{y0}^T \tilde{D}_{yu,c} \end{bmatrix} K_u\left[\star\right] \prec 0,$$

$$\begin{bmatrix} \tilde{A}_d^T P_d + P_d \tilde{A}_d & P\tilde{C}_{z,d}^T & P\tilde{C}_{y,d}^T k_{y0} \\ \star & 0 & 0 \\ \star & 0 & -\gamma^2 I \end{bmatrix} + \lambda_d \begin{bmatrix} \tilde{B}_{w,d} \\ \tilde{D}_{zw,d} \\ k_{y0}^T \tilde{D}_{yw,d} \end{bmatrix} M_d\left[\star\right] + \begin{bmatrix} \tilde{B}_{u,d} \\ \tilde{D}_{zu,d} \\ k_{y0}^T \tilde{D}_{yu,d} \end{bmatrix} K_u\left[\star\right] \prec 0,$$

$$0 \preceq K_u \preceq I,\ Q \succeq 0,\ P_d \succ 0,\ \lambda_c \succ 0,\ \lambda_d \succ 0.$$

for $k = 1$ to $n_u - 1$ **do**

  $j = 0$

  $K_u^\star = \mathcal{P}_{\Gamma_{\text{rank}}^{n-k}} K_u$

  while $\frac{|K_{u_{j+1}}^\star - K_{u_j}^\star|}{|K_{u_j}^\star|}$ > threshold **do**

    Solve the following optimization problem, for λ_c, λ_d, P_c, Q, P_d, S, K_u:

$$\underset{P_d,\, K_u,\, P_c,\, Q,\, S,\, \lambda_c,\, \lambda_d}{\text{minimize}} \quad \text{trace}\,(S)$$

s.t.:

$$\begin{bmatrix} \tilde{A}_c^T & \tilde{C}_{z,c}^T & \tilde{C}_{y,c}^T k_{y0} \\ 0 & 0 & 0 \\ I & 0 & 0 \end{bmatrix}^T \Xi\left[\star\right] + \begin{bmatrix} 0 & 0 & 0 \\ 0 & 0 & 0 \\ 0 & 0 & \beta^2 I \end{bmatrix} + \lambda_c \begin{bmatrix} \tilde{B}_{w,c} \\ \tilde{D}_{zw,c} \\ k_{y0}^T \tilde{D}_{yw,c} \end{bmatrix} M_c\left[\star\right] - \begin{bmatrix} \tilde{B}_{u,c} \\ \tilde{D}_{zu,c} \\ k_{y0}^T \tilde{D}_{yu,c} \end{bmatrix} K_u\left[\star\right] \prec 0,$$

$$\begin{bmatrix} \tilde{A}_d^T P_d + P_d \tilde{A}_d & P\tilde{C}_{z,d}^T & P\tilde{C}_{y,d}^T k_{y0} \\ \star & 0 & 0 \\ \star & 0 & -\gamma^2 I \end{bmatrix} + \lambda_d \begin{bmatrix} \tilde{B}_{w,d} \\ \tilde{D}_{zw,d} \\ k_{y0}^T \tilde{D}_{yw,d} \end{bmatrix} M_d\left[\star\right] + \begin{bmatrix} \tilde{B}_{u,d} \\ \tilde{D}_{zu,d} \\ k_{y0}^T \tilde{D}_{yu,d} \end{bmatrix} K_u\left[\star\right] \prec 0,$$

$$\begin{bmatrix} S & K_u - K_u^\star \\ K_u - K_u^\star & I \end{bmatrix} \succeq 0,$$

$$0 \preceq K_u \preceq I,\ Q \succeq 0,\ P_d \succ 0,\ \lambda_c \succ 0,\ \lambda_d \succ 0.$$

    $K_{u_{j+1}}^\star = \mathcal{P}_{\Gamma_{\text{rank}}^{n-k}} K_{u_j}$

    $j = j + 1$

  end while

end for

Find k_u as the left singular vector corresponding to the largest singular value, from the singular value decomposition $K_u^\star = USV^T$.